Michaelsen and Storetvedt, 2026. Mongolian Geoscientist 31 (62)
https://doi.org/10.5564/mgs.v31i62.5643

Mongolian Geoscientist

Review paper

Wrench tectonics and major environmental changes across the Permo-Triassic boundary recorded in a coal-bearing basin, South Mongolia

Per Michaelsen[1*] and Karsten M. Storetvedt[2]

[1]*Geoscience Center, School of Geology and Mining Engineering, Mongolian University of Science and Technology, Ulaanbaatar, 14191, Mongolia*
[2]*Geophysical Institute, University of Bergen, 5020 Bergen, Norway*

**Corresponding author:* perm@must.edu.mn, *ORCID:*0000-0003-4075-8943

ARTICLE INFO

Article history:

Check for updates

Received: 10 June, 2026
Revised: 09 July, 2026
Accepted: 18 July, 2026

ABSTRACT

Syn-tectonic deposition of the Late Permian coal-bearing Yamaan Us Formation of the Tsagaan Tolgoi sub-basin, South Mongolia, was abruptly terminated due to the most severe mass extinction in Earth's history. As the principal dying out events have occurred simultaneously with tectono-magmatic upheavals characterizing major geological time boundaries, the Permo-Triassic sedimentary fill of the sub-basin is a characteristic example of Earth's pulse-like history. It is considered axiomatic that the pulsing globe is triggered by internal outgassing, with related mass reorganization, episodic dynamic implications, and inertia-based moderate wrench tectonics. In this development scheme, the moderate tectonically deformed sub-basin, c. 1,000 m thick, records a dramatic transition from humid fluvio-paralic coal-forming environments characterized by abrupt facies changes during the Late Permian, to arid barren terrestrial conditions during the Early Triassic. Coal ash composition analysis shows a marked increase in average SO_3 content from 2.09% in the thick basal seam to 6.88% in the topmost, which might be coupled to pulses of toxic gas exhalation - in this case perhaps mainly from the contemporary Siberian Traps. Very rare fire-scarred fossil wood fragments, discovered in the topmost part of the coal measures, probably resulted from wildfire- caused by outgassed methane ignited by lightning. Preliminary analysis of fossil wood growth rings shows significant internal variation in annual ring thickness and overall decrease upwards towards the End Permian Mass Extinction, indicating critical stress in plant ecosystems linked to complex toxic haze, acid rain and hypoxia. However, the sedimentary record shows no spatial-temporal diminution of coal seams prior to the End Permian Mass Extension indicating abrupt termination of peat mire deposition.

Keywords: South Gobi Basin, coal measures, basin analysis, wildfires, End Permian Mass Extinction

INTRODUCTION

The fault-bounded Permo-Triassic Tsagaan Tolgoi sub-basin (TTSB) in southern Mongolia, c. 115 km north of the Chinese border, was situated along the northern shores of the South Mongolian Seaway during Late Permian times (Manankov, 1998, 1999, 2012; Manankov et al., 2006). Similar Permian coal-bearing basins in Mongolia have developed as isolated units often sandwiched between wrench faulted basement blocks (Michaelsen and Storetvedt, 2023; 2024, Storetvedt and Michaelsen, 2024; Michaelsen and Demberelsuren, 2024). The reason for this structural subdivision is that throughout the Palaeozoic, an upper crustal mantle - with its steeply dipping northwest- and northeast-oriented orthogonal fracture network - was subject to episodic clockwise inertia-triggered wrench deformation (Michaelsen and Storetvedt, 2023). During the Palaeozoic, seawater volume was moderate, with a cosmopolitan fauna living in epi-continental conditions (Peters and Gaines, 2012; Storetvedt, 2026). Thus, a plane or slightly undulating continental surface must have existed when the first water pulses of any importance, in Cambro-Ordovician times, were expelled from the interior, associated with an explosion of higher life forms. Throughout the rest of the Palaeozoic, irregular moderate thinning of the pan-global continental crust led to formation of epicontinental basins (Ruditch, 1990; Storetvedt, 2003/23, 2025, 2026). Towards the end of the Permian, relatively unaffected crustal masses experienced its deepest Palaeozoic regression (Hallam, 1992). In consequence, the once widely covered epicontinental seas of Central Asia were reduced to narrow shallow seaways along which the economically important Mongolian coal-bearing basins developed (Storetvedt and Michaelsen, 2024). Furthermore, the deep regression, which culminated at the Permian-Triassic boundary (PTB), coincided with the largest extinction in Earth's history (Retallack, 1995; Hongfu et al., 2001; Michaelsen, 2002; Jasper et al., 2016; Li et al., 2016; Shen et al., 2018; Cui et al., 2021; Lu et al., 2022; Song et al., 2022; Jiao et al., 2023; Zhang et al., 2023; Ragon et al., 2025). The oscillatory deep regression - associated with accelerated regional crustal thinning and isostatic subsidence - appears to have been primarily localized to the present-day Pacific (Ruditch, 1990; Storetvedt, 2025). Crustal development was apparently caused by subcrustal eclogitization with associated gravity-driven crustal loss to the upper mantle (Austrheim, 1987; McMillan et al., 2025), a process that was in turn closely linked to the release of gases and aqueous fluids - on land and in the seafloor (Michaelsen and Storetvedt, 2023). In this process, it is likely that the associated Late Permian tectonic phase triggered widespread gas-driven volcanic activity with explosive cratering, particularly in regions of ongoing crustal thinning and isostatic subsidence.

On this background, we infer that the development of the small-scale TTSB is closely connected to the physical course of the Earth - a long-lasting, slow and episodic degassing history towards thermochemical equilibrium. In this process, episodic changes of the planet's moment of inertia have become the principal dynamo-tectonic driver for all pulse-like geological processes - as well as functioning as a hydraulic pumping device for ejecting water, metals and abiotic hydrocarbons to surface levels (Storetvedt, 2003/23, 2026; Storetvedt and Michaelsen 2024). In the degassing theory, both marine and terrestrial biotic crises are simultaneous and caused by toxic gases and fluids released through the surface both on land and in the seabed - including sulphur dioxide, hydrogen sulphide, hydrogen halides and carbon monoxide which are poisonous and combustible. In addition, the marine environment suffered from anoxia while the continents must have been subject to a complex, partly toxic, haze - expectedly giving rise to a combination of reduced solar radiation, lowered surface temperatures, poorer growing condition, wildfires and soot layers (Augland et al., 2019; Cai et al., 2021; Dal Corso et al., 2022, 2024; Jiao et al., 2023; Hua et al., 2024; Xie, 2024; Bhattacharya et al., 2025). By using outgassing as the axiomatic basis for the Earth's evolution, with its various crustal manifestations, dynamical records, and surface products, it appears that a "first-order" observation-prediction-verification chain may be underway (Storetvedt, 2003/23). This implies that Mongolia's tectono-magmatic history, its natural resources, and environmental records are sequential in situ products of the way the Earth works (Michaelsen and Storetvedt, 2023; Storetvedt and Michaelsen, 2024).

WRENCH TECTONICS OF THE TTSB

In a wider perspective, Mongolia's tectonic history constitutes a series of inertia-driven transpressive - transtensive reactivations of the omnipresent orthogonal and steeply dipping fracture/fault system - building up superimposed tectono-magmatic successions in situ. In southwestern Mongolia, the cutting-across of the late Ordovician palaeoequator led to substantial reactivation of the steeply dipping orthogonal fracture/fault system, as well as paving the way for the overall geological history of Mongolia. The Late Ordovician palaeo-equator ran along the Altai belt (Michaelsen and Storetvedt, 2023).

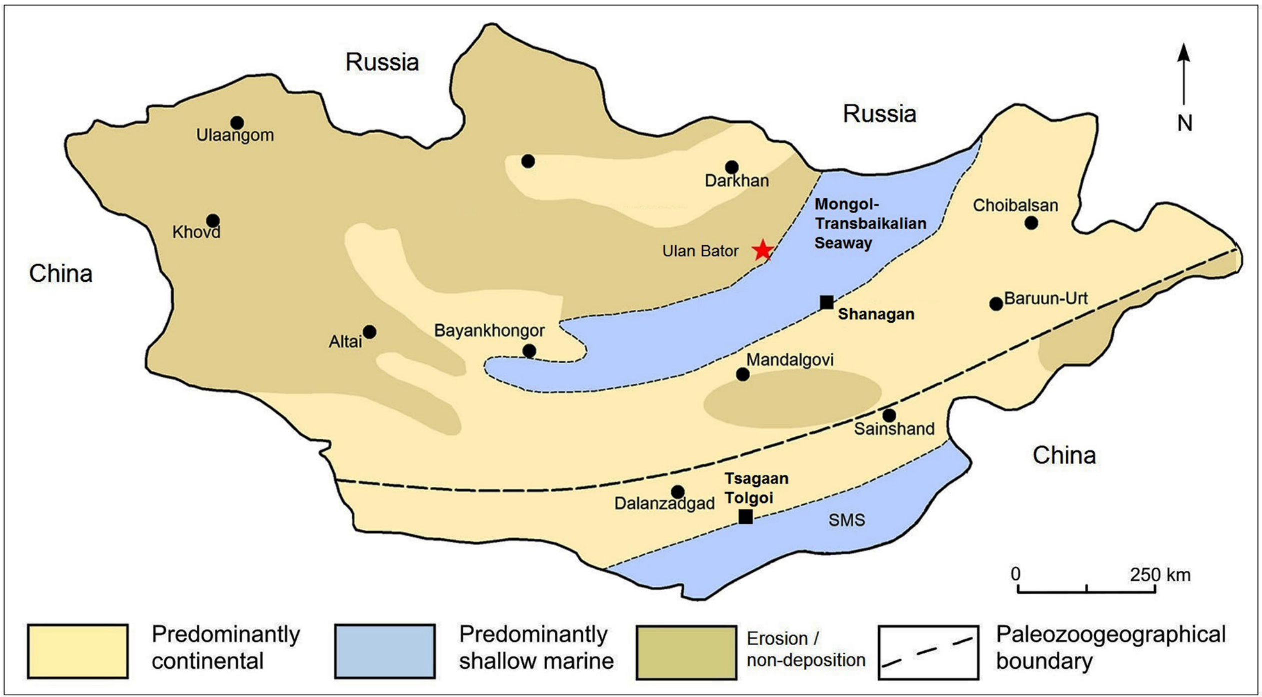

Fig. 1. Generalized spatial distribution map of Permian sedimentary strata in Mongolia showing location of the Tsagaan Tolgoi study area (modified from Manankov et al., 2006).

During this time a significant part of Mongolia belonged to the northern palaeo-hemisphere, where the general inertial effect is clockwise. This tectonic situation has persisted, but with gradually decreasing strength, resulting from the palaeoequator having stepwise moved away from Mongolia - towards today's equator where the palaeoequators form intersections at c. 90°E and W respectively (Wegener, 1929/66; Storetvedt, 1990). The Late Ordovician wrenching of an upper crustal layer gave rise to predominantly different tectonic results between western and eastern Mongolia. While the western part was dominated by transpression and high strain zones, along the basal NW-striking fault set, eastern Mongolia was overshadowed by transtension along the orthogonal (NE-striking) planar fault system (Michaelsen and Storetvedt, 2023). During the Palaeozoic, the orthogonal fault network was repeatedly inertially reactivated during which the (palaeo) latitude-dependent westward torsion led to tectonic interaction between the two fault sets. This "loop chain" interaction is likely the cause of the south-facing Mongolian tectono-topographic arc, as well as the corresponding shape of the Mongol-Transbaikalian Seaway (Fig. 1). In southern Mongolia, however, the interaction between the two perpendicular fault sets became unusually sharp, causing the prevailing tectonic grain to take on an E-W orientation - along which the elongate trapezoidal-shaped Late Permian TTSB developed (Fig. 2). In the latest Palaeozoic, the palaeoequator (along which the inertial effect is at its maximum) was more distant from Mongolia, running across north-central India. One would expect therefore that the related all-Mongolia inertial wrenching would be reduced. On the other hand, the pronounced crustal break-up interaction in south Mongolia and the significant earthquake activity notably in southwestern regions of the country (Sodnomsambuu and Klyuchevskii, 2017) - the latter probably being a persistent degassing phenomenon, would have led to long-lasting but variable tectono-magmatic superimposition. In previous articles (Michaelsen and Storetvedt, 2023, 2024; Storetvedt and Michaelsen, 2024) we have referred such cases to upper crustal inertia-twisted decks - for which the (sub)horizontal disconnected crustal 'cards' are due to a combination of the, by now, abundant evidence of hydrous fluids in the continental crust - as evidenced in the deep Kola (Kozlovsky, 1984) and the KTB (Kontinentale Tiefbohr), Germany (Ito and Zoback, 2000) boreholes, with attendant supercritical water-produced mud, serpentinization, and chlorite development. As we shall see below, the TTSB is another and not

Fig. 2. A) Advanced spaceborne thermal emission and reflection radiometer (ASTER) image of the TTSB district shows that the primordial orthogonal fault network is clearly visible - despite the strong wrench tectonic deformation of the upper regional crust during the Permian. Moderate clockwise rotation (top right) is shown for a block covered with Carboniferous rocks. B) Rose diagram of reconciled in-situ stress indicators obtained from the study area

unexpected example where the Lower-Middle Paleozoic tectonic grain is rotated, variably warped and partly cut by a transverse regional wrench fault (Fig. 2) - compressing the Permian-Triassic sub-basin.

The elongate fault-bounded TTSB, which extends E-W for c. 22 km shows gradual thinning eastwards - with width varying from c. 4 to 1.5 km. To the north, the sub-basin is bounded by Carboniferous basement rocks, and partly to the south, and on side-wall faults to the west, by silicious volcanics (Fig. 3). The main structural feature is a broad and gently eastward dipping syncline, modified at several levels by smaller-scale folding and faulting. The syncline axis reflects the regional trend of the South Gobi Basin - consisting of a series of E-W oriented transtensional sub-basins. The eastern sector of the TTSB is masked by modern sediments with only sporadic Permian outcrops. Therefore, the present paper focuses on the western part where steeply dipping Late Permian coal measures are well exposed in a c. 4 km² large area adjacent to the sidewall fault. A thick sequence (up to 50 m in places) of reworked quarts-rich volcanic material - a muddy and conglomeratic rock, forms the base of the Late Permian coal measures (i.e. the proposed Tsagaan Tolgoi Tuff Member). It is likely that the TTSB syncline began its subsidence before the volcanic event, with mud production through the breakdown of basement rocks - a disintegration product of the release of high-pressure supercritical aqueous fluids (Dimitrov, 2002; Hovland et al, 2006), primarily along the central fault zone.

The most important tectonic event, affecting the sub-basin and its surroundings, was however a transverse northern palaeo-hemispherical clockwise wrench rotation (Fig. 2), which probably occurred concurrently with the volcanic stage. It is important to point out that in a crustal “deck of cards” condition in the Earth’s crust (Michaelsen and Storetvedt, 2023), based on findings from deep continental drilling (Kola and KTB; Kozlovsky, 1984, Ito and Zoback, 2000), the need for inertial forces during small-scale tectonic rotations may be moderate to small. During this regional inertia-triggered event (possibly a precursor of the End Permian Mass Extinction (EPME) bio-catastrophic event), the

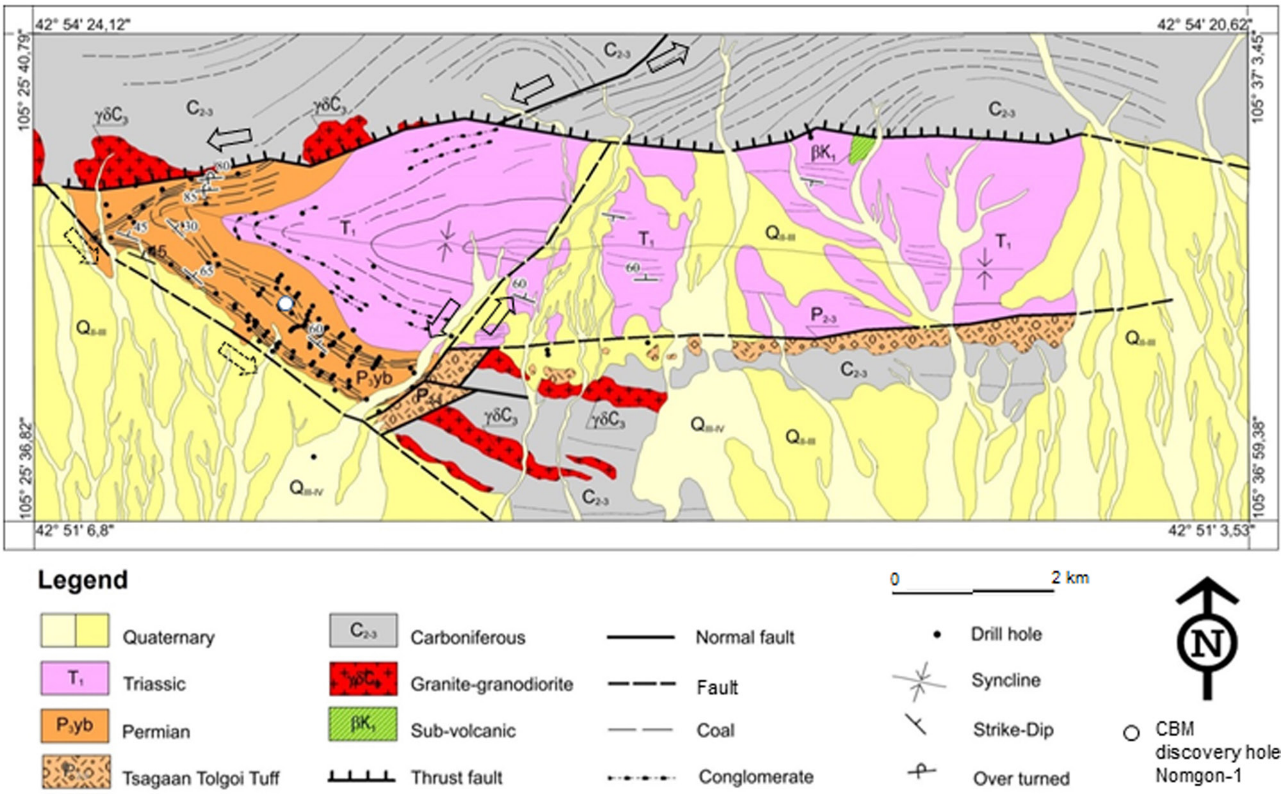

Fig. 3. Generalized geology map of the western part of the TTSB showing location of drill holes, bedding, main faults and stratigraphic units. The present margin of the sub-basin is a structural/erosional boundary and does not accurately reflect the more extensive depositional basin

northern TTSB boundary became transpressive, while the southern faulted boundary underwent transtensive conditions. This difference in tectonic regime is apparently the reason why the predicted explosive volcanism is basically concentrated on the southern margin. During this tectono-volcanic phase, the western sub-basin was most strongly affected - cutting the basin into a western and an eastern subdivision by a left-lateral SW-NE oriented shear zone (Fig. 3). This tectonic disturbance is apparently the reason why the proposed Tsagaan Tolgoi Tuff Member (TTT in Figs. 4 and 5) of the southwestern sector is the thickest of its kind in the TTSB multiphase development. It is noted that the NE trending sinistral wrench fault has some expression on gravity maps, with high gravity values to the west of the fault (i.e. the sedimentary depocenter) and lower values to the east. This suggests the sub-basin experienced syn-tectonic deposition during Late-Permian to Early Triassic times as we will see in the ensuing Facies Analysis and Depositional Environments sections.

In the inferred transtensive circumstances, the Late Permian peat-forming vegetation, which colonized the mud-dominated volcanics, might have benefitted from carbon-rich gases upwelling along the fault-bounded south-western margin. Furthermore, the sub-basin constitutes a central steeply inward-dipping syncline, presumably following along a principal fault zone of the regional tectonic grain. Therefore, to account for the subsidence of the basin, a reasonable explanation is that the basement rocks have undergone significant disintegration to mud along the central fault zone. In this process, the rising high-pressurized gases and supercritical fluids, along with the south-westerly sliding effect, transported the muddy component away from the central fault zone towards the transtensional southern border. Consequently, supercritical aqueous fluids were both the producer and transporter of the sludge that was blown out along the southern TTSB border - together with silicic mud and fragments of pure degassing-produced quartz (Hunt et al., 1992). The volcanic eruption centers along the basin's southern border are well demonstrated by whitish hills in the image of Fig. 4A. On the planar marshy surface, the mud fraction would easily spread out as flood basin deposits. The Permo-Triassic bedding generally dips around 60-70° throughout the TTSB, indicates that the basin must have been affected by significant compression instigated by the inferred superimposed inertia-instigated clockwise deformation. As will be outlined below, we suggest that originally the Triassic sequence probably was much thicker than suggested from its present depth - with considerable erosion during the transtensive tectonic phase. In that event, the northwestern end of the Late Permian coal-bearing sequence has been inverted, as it means that the tectonic deformation of the TTSB tightens westward. This indicates that the pivotal region of the regional upper crustal inertial rotation may lie only a short distance to the west (Figs. 2-3).

MATERIALS AND METHODS

This research is based on field work conducted sporadically from 2010 to 2026 on the sedimentary succession preserved within the TTSB, including detailed mapping of the entire sub-basin during 2018-2020. A total of 228

Fig. 4. A and B) outcrop images of the TTT from the southwestern flank of the sub-basin looking north, C) photomicrograph of thin-section TTT03 showing laminated fine, clay-rich matrix with abundant quartz crystal fragments (i.e. crossed polarizers), and D) image looking NNE of the conformable contact between the TTT and overlying deposits. Note the elevated northern Carboniferous basement in the background behind the distinct brownish-orange-colored Jurassic strike ridges in the depocenter.

selected field stations were recorded (position, strike/dip, stratigraphy, lithology, sedimentary structures, fossils, stress indicators such as slickenside structures and photo documented). This was followed by coalbed methane (CBM) target generation work (Channon and Young, 2019) for Elixir Energy and subsequent deep CBM drilling supervision. During the CBM core logging program, event signatures, lithofacies contacts, sandstone attributes, biogenic features, sedimentary structures, coal characteristics, gas bubbles and cleats were given special attention. The CBM drill cores from the exploration program are secured in wooden boxes at the senior author's Camp Slejpner in Dalanzadgad, South Mongolia. The classical terminology of Wentworth (1922) was used for grain-size subdivisions, whereas the standard scheme of Folk, (1974) was used for admixtures. Terminology of sedimentary structures was obtained from Collinson and Thompson (1982), and Miall (2006, 2022). Trace fossil intensity was based on Bann and Fielding (2004). This study draws on 1) a new coal quality database encompassing 69 coal samples obtained from outcrops of seams 1, 2, 4, 5, 6 and 7; 2) recent coal seam gas and coal thickness data from Elixir Energy, continuously disclosed to the Australian Stock Exchange and as such in the public domain, and 3) historical coal quality data by South Gobi Resources which were continuously disclosed to the Hong Kong Stock Exchange in numerous announcements. Recent field work during 2025-2026 focused on sedimentary facies analysis of outcropping Late Permian coal measures in the western sector, the Jurassic system in the depocenter of the sub-basin, and sampling for age dating. Paleocurrent data were collected from sandstone outcrops with trough-cross stratification (TCS) across the PTB. Furthermore, a total of 11 samples of the TTT were attained from outcrops over a strike length of 9,6 km along the southern flank of the sub-basin, with 11 thin sections studied at Mongolian University of Science and Technology. Numerous silicified tree trunks were collected from the Late Permian coal measures and the Permo-Triassic transitional zone for rudimentary growth ring analysis, partly using the methods detailed by Taylor and Ryberg, 2007. The sampling method for the new coal outcrop database was non-uniform: A) thicker coal seams (i.e. +1 m) were sampled at 1 m intervals, whereas B) thin seams (i.e. <1 m) were sampled at 0.3m intervals. Prior to sampling, weathered, oxidized coal and surface debris were removed to expose a fresh, clean face, typically 30-50 cm deep. Double plastic bags were used for each sample which was sealed to retain moisture. Sample number, seam number, and sample depth were written on all inside bags. Coal quality samples for each seam interval were compiled in larger marked and sealed double plastic bags. All samples were subsequently boxed and personally transported to the Energy Resources Central Laboratory in Tsogttsetsii, South Gobi, for processing, preparation of briquettes, maceral group composition analysis, measurement of vitrinite reflectance and proximate analysis. The ISO 7404-2 (2009) standard was followed for the preparation of briquettes. ISO 7404-3 (2009) was used to determine maceral group composition, whereas ISO 7404-5 (2009) guidelines were followed for vitrinite reflectance measurements. The maceral group composition analysis was carried out on prepared briquettes under reflected light using a LEICA DM4P polarization microscope (Demberelsuren et al., 2023). The spacing between the counts was maintained at 0.2 mm and 500 counts were taken on each sample. The ICCP (International committee for Coal and Organic Petrology) classification system 1994 was used to distinguish maceral groups of vitrinite, whereas the liptinite classification system from 1998 and 2001 were used to distinguish inertinite and the system developed by Pickel et al. (2017) was used to distinguish liptinite. Clay, carbonate, silica, pyrite and other minerals were determined. The vitrinite reflectance was measured on a FOSSIL #10 726 microscope with a LEICA DM4P camera (Demberelsuren et al., 2023). The examination was conducted using a 50x magnification ocular lens under Zeiss oil immersion (518 N). The random vitrinite reflectance was measured from 50 to 100 points in each sample. The mean random vitrinite reflectance values were then calculated applying the FOSSIL #10 computer program. Proximate analysis was analyzed on each sample to determine moisture, ash, volatile matter, and sulfur content. MNS GB/T 212:2015 was used to determine moisture, ash yield, and volatile matter content, and MNS ISO 351:2001 was used to determine the sulfur content.

Stratigraphic framework of the Tsagaan Tolgoi succession

The lithostratigraphic components of the TTSB are summarized in Table 1 and described briefly in the following, with the focus on the Late Permian Yamaan Us Formation (YUF), established by Orolmaa et al. (1999), who estimated the sedimentary succession to be up to 1,500 m thick. This study has revised the true thickness of the sub-basinal fill to be up to c. 1,000 m, and c. 550 m for the coal-bearing YUF, based on recent mapping work coupled with observations from the latest deep CBM drilling. The Changxingian age for the YUF is well established from palynomorphs and Angaran compression floras by a succession of previous workers (Durante, 1976; Vakrameev et al., 1986: Burenkhuu et al., 1995; Zinniker and Badarch, 1997: Orolmaa et al., 1999: Durante and Luvsantseden, 2002; Uranbileg, 2003; Aristov, 2005; Johnson et al., 2007; Cai et al., 2022, 2023, 2024; Michaelsen and Storetvedt, 2024). However, no absolute age dating has been reported given the very rare nature of tuffs and absence above seam 3. The coal-bearing part of the YUF is estimated here to have a maximum true thickness of c. 550 m in the western depocenter, with gravity maps indicating eastward thinning coupled with the narrowing of the sub-basin. Results from recent mapping show the formation is sporadically exposed over an east-west strike length of c. 22 km.

The base of the coal measures is characterized by an up to c. 50 m thick whitish stratigraphic marker bed, locally known as the “Tsagaan Tolgoi Tuff” (TTT, Fig. 5), which is proposed here to be formally elevated to stratigraphic member status given the important marker bed characteristics and lateral continuity. Recent mapping shows the TTT sporadically outcrops over a c. 22 km strike length along the southern margin of the sub-basin, and along the NW oriented sidewall fault to the west, with only rare outcrops along the northern margin (Fig. 3). The unit is best exposed in the south-western part of the sub-basin where it forms a c. 50 m high whitish hill which gives the sub-basin its name of Tsagaan Tolgoi (“white hill”) Fig. 4A, proposed here as type section. The unit is very noticeable in aerial photographs and LANDSAT images (Fig. 2). A total of 11 TTT samples were attained from outcrops along the southwestern margin over a strike length of 9.6 km (Appendix Table 1). Analytical work reveals the volcanic sediments are acidic in composition, with secondary quartz developed along laminae interfaces (Fig. 4C). Recent CBM drilling in the western sector shows the TTT is inter-bedded with thin coal beds of the basal seam 0 horizon (Fig. 5), and as such should be included as a basal member of the YUF. The TTT unit is considered here to represent reworked deposits of mud volcanoes or fissures associated with inertia-driven transtensive reactivation of deep-seated primordial fault zones (Michaelsen and Storetvedt, 2023, 2024). It is noted that mud

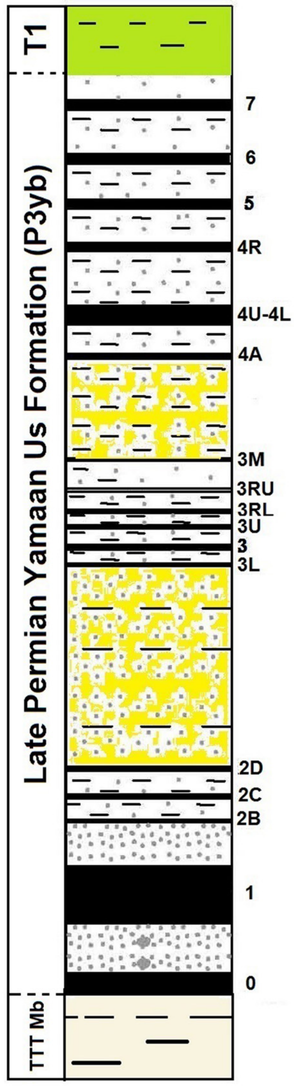

Fig. 5. Generalized lithostratigraphic log of the Permo-Triassic sedimentary succession of the TTSB with informal member and coal seam nomenclature.

Table 1. General overview of the stratigraphic units within the Tsagaan Tolgoi study area and their main attributes. Red horizontal lines indicate angular unconformities

Chronology	Lithostratigraphy		Approximate True Thickness (m)	Fossils	Paleoclimatic Indicators	Sedimentary Structures	Environmental Conditions	Depositional Systems	Tectonic Regime
	Formation	Sub-Group							
Neogene		N	50	Barren	Redbeds	Horizontal and disturbed bedding. Trough-cross stratification	Relatively humid	Fluvio-lacustrine. Rapid sediment dispersal with poor sorting	Transpressional regime with significant regional uplift, erosion and rapid sediment dispersal
Jurassic (?)		J_2	100	Compression floras (mosses of *Tricostium, Yamanusia, Atrichites* and *Palaeosyrrhopodon)*. Abundant insects of protorthopterous Chauliodítidae *and* mayfly nymphal exuvia	Mosses indicating a relatively humid climate	Trough cross-stratification and horizontal bedding.	Humid. Possibly episodic runoff regime where mosses had time to colonize the landscape inbetween fluvial sediment dispersal	Fluvial	Short lived transtensive event with relatively minor subsidence in western deposcentre
Early Triassic		T_1	250	Barren	Barren greenish siltstone. Carbonate nodules	Horizontal bedding and trough-cross stratification. Concretions	Relatively arid desolate conditions	Fluvial	Transtension
Late Permian	Yamaan Us	P_3yb	550	Abundant leaf imprints of Angaran flora esp. *Cordaites Sulcivius* and *Lepidophyte and Cicadocea (Guramsania hosbairica). Secrospiroxylon tolgoyensis.* Rare *Connulariid* at base	Siderite horizons (particularly well developed in lower section). Cai et al. (2022) described a deciduous conifer that lived in a seasonal, temperate, and wet climate with relatively short growing seasons	Horizontal, lenticular, wavy and disturbed bedding. Trough-cross stratification and ripple cross lamination. Coaly traces. Bioturbation *(Skolithos, Planolites* isp. and inclined structures).	Common base-level changes. Temperate humid climate with short growing season	Long lived peat mire ecosystem developed on lower coastal plain, inter-fingering with near shore depositional system	Reactivation of subvertical primordial wrench faults. Transtension
		Tsagaan Tolgoi Tuff Member	50	Coal-bearing	A relatively long lived lacustrine system in the southwestern sector suggest a humid setting	Horizontal bedding and trough-cross stratification	The occurrence of thin coal beds indicate episodic flashy runoff where plants had brief windows to colonize the landscape	Fluvio-lacustrine	

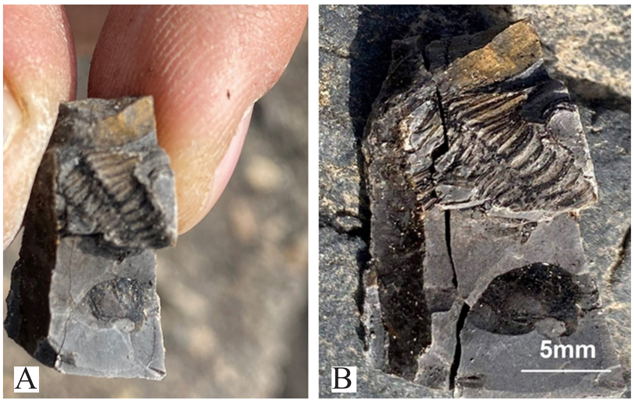

Fig. 6. Field images of the *Conulariid* fossil fragment discovered at the base of the coal measures.

volcano deposits usually occur as linear features (Dimitrov, 2002; Hovland et al., 2006) and thought to be deposited due to the over pressure of muds at depth caused by a slowly degassing Earth.

The YUF is characterized by a total of eight coal horizons (numbered 0 - 7), distributed in three coal-bearing zones (upper, middle and lower). The three coal zones are separated by two c. 75-241 m thick clastic packages (Fig. 5). The lower coal-bearing zone includes seam horizons 0, 1 and 2, the middle zone contain seam horizon 3, whereas the upper zone includes seam horizons 4 to 7. A very rare *Conulariida* fragment (Fig. 6) was recently discovered within the clastic sequence between seams 0 and 1 along the northern flank of the sub-basin at 42°52'32.64"N/105°27'45.56"E. Such fossils are particularly valuable for reconstructing ancient water temperatures, seafloor oxygen levels, basin migration patterns and water energy (e.g. Van Iten, 1991). During the Permian period, the paleogeographic distribution of these fossils strongly indicates a preference for cooler waters (Waterhouse, 1979). The boundary between the Late Permian coal measures and the conformably overlying Early Triassic sandstone dominated formation is transitional over a c. 50 m thick interval (Fig. 7). This stratigraphically important

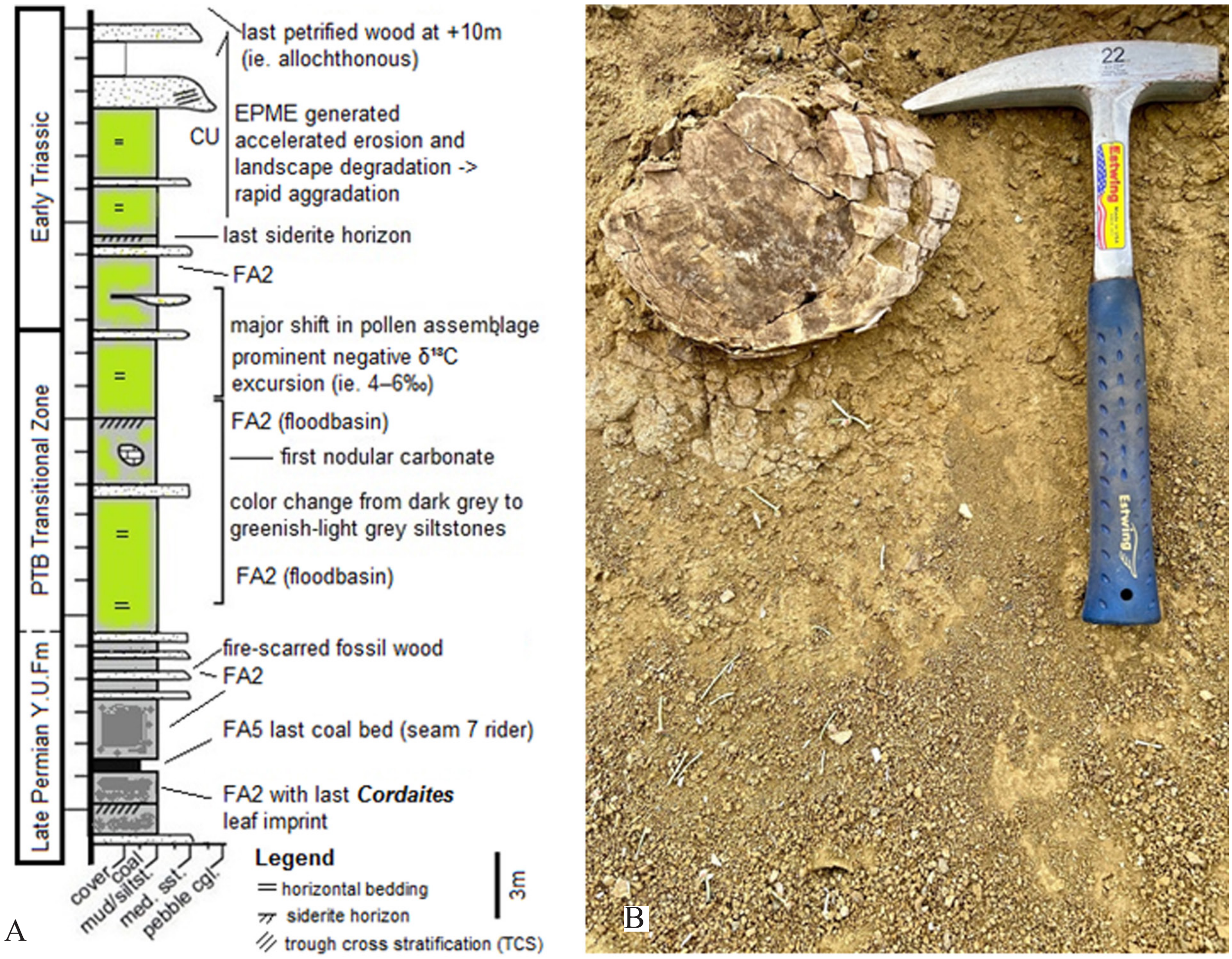

Fig. 7. A) Measured section by Johnson et al. (2007) across the Permian-Triassic boundary at Tsagaan Tolgoi (text for discussion - modified from Johnson et al., 2007), and B) allochthonous uppermost fossil wood fragment preserved within in greenish PTB transitional zone

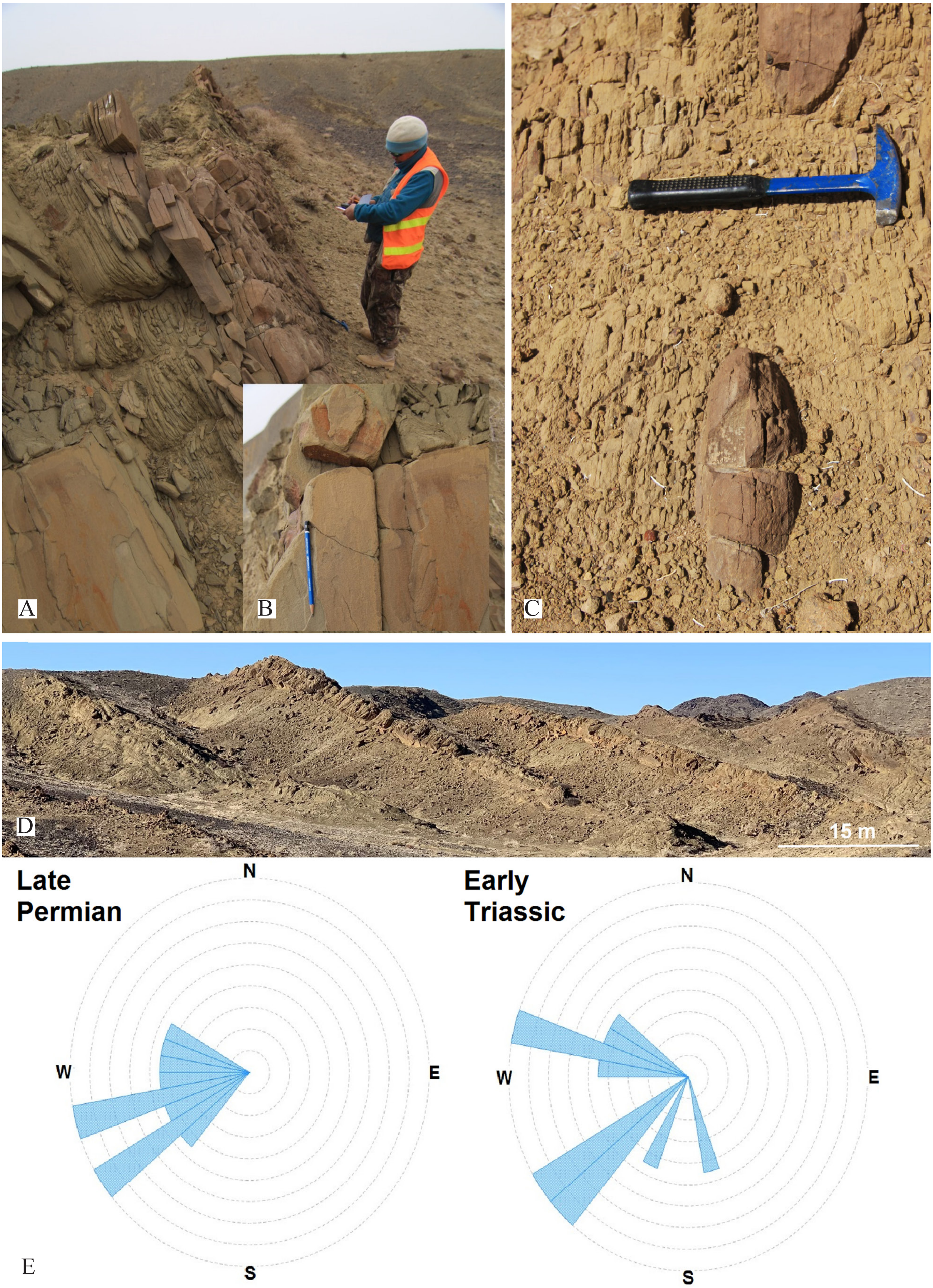

Fig. 8. A-B) Lower Triassic greenish barren sediments and C) calcareous nodules indicating arid desolate conditions after the PTB, D) well developed Early Triassic Milankovitch cyclothems, and E) Permo-Triassic paleocurrent data showing persistent westward sediment dispersal across the PTB

interval was well documented by Johnson et al. (2007), which holistically established the PTB within the zone based on Carbon isotope data, palynology, macroflora and sedimentological observations. Importantly, Johnson et al. (2007) reported characteristic Late Permian pollen genera such as *Cordaitina, Florintes, Potonieisporites and Neoraistrickia*, whereas Early Triassic and transitional zone species comprise *Lueckisporites virkiae, Lundbladispora sp.,* and *Taenisporites* sp. Notably, *Taeniate*-striate *bisaccate* is typically associated with evaporites and more arid conditions. The transitional interval is dominated by siltstone in the lower part, coarsening upwards with an increase of medium-coarse grained sandstone beds. The sediments color changes from greyish to greenish, calcareous nodules measuring up to 1.8 m across appear, and siderite horizons gradually disappear (Fig. 7). Additionally, Johnson et al. (2007) reported a prominent negative organic $\delta^{13}C$ isotope ratio excursion of 4-6‰ coincident with changes in lithology and pollen assemblage (Fig. 7). The siderite horizons are relatively thin at 12-16 cm compared with the typical 25-70 cm within the underlying coal measures. Rare allochthonous petrified wood trunks (Fig. 7B), measuring up to 24 cm across, occur in places.

The conformable overlying Early Triassic barren sediments were estimated to have a maximum thickness of c. 250 m within the western depocenter where they are well exposed and dominated by fine-coarse grained sandstone and greenish siltstone beds with common calcareous nodules (Fig. 8). The transitional Permo-Triassic coarsening upward zone (Fig. 7) is overlain in by a fluvial succession of up to nine fining upward sequences with individual thickness measured during field work at c. 7-16 m (Fig. 8D). Basal matrix-supported conglomerate units show sub-angular to well-rounded pebble size clasts up to 4.1 cm in length and generally overlain by pebbly coarse-medium grained sandstone beds, showing textural and compositional immaturity, fining upwards to greenish siltstone. Sedimentary structures are dominated by TCS with subordinate horizontal bedding (Fig. 8B). Paleocurrent measurements from TCS were acquired from medium-grained sandstone beds, indicating westward sediment dispersal (Fig. 8E). Field observations show the Early Triassic sediments are unconformably overlain by an up to c. 100 m thick coarse grained Upper Jurassic fluvial sequence sporadically preserved along the synclinal axis in the western depocenter (Table 1, Figs. 2, 5D). Compression floras of the mosses *Tricostium, Yamanusia, Atrichites* and *Palaeosyrrhopodon* were reported from the unit by Ignatov and Shcherbakov (2011, Table 1), with Tricostium formerly described from the Upper Jurassic (Ignatov and Shcherbakov, 2011). Previously Shcherbakov (2008) reported abundant insects of *protorthopterous Chauliodititidae* and mayfly *nymphal exuvia*, from the same unit, and suggested a Triassic age. However, results from recent mapping agree with the data by Ignatov and Shcherbakov (2011). The distinctly colored Upper Jurassic sediments form prominent strike ridges within the western part of the study area, with a maximum length of c. 380 m (Fig. 5D). The Paleozoic and Mesozoic sediments are in places overlain by semi-consolidated Neogene red beds estimated to be up to c. 50 m thick (Table 1). The primordial pan-global orthogonal wrench tectonic rupture system is expressed by numerous linear NE to NW oriented ephemeral drainage systems within the study area (Fig. 3). Due to the persistent wrench tectonic history, the old rupture system has been transferred into ever younger surface strata.

RESULTS

Facies analysis of the coal-bearing YUF (P_3yb)

The results show the Late Permian YUF is characterized by six coal-bearing alluvial to shallow marine facies associations (FA), with their architectural and temporal relationships allowing for a preliminary reconstruction of the coal-bearing depositional system. The six facies are summarized in Table 2 and briefly described below.

Facies association 1 (FA1): fluvial channels

FA1 comprises light gray, fine to very coarse-grained pebbly sandstone organized as erosional-based ribbons and sheet-like multi-story bodies. Rip-up clasts ranging to 8.1 cm in length are common. Two sub-facies of genetically related deposits with significantly different characteristics occur: Sub-facies FA1a comprise

Table 2. Summary of the six sedimentary facies associations recognized within the coal measures.

Facies Association	Lithology	Sedimentary Structures	Geometry	Fossils	Other Features	Depositional System
1	Poorly sorted medium-very coarse grained pebbly sandstone and sub-angular to sub-rounded extraformational conglomerate. Medium - thickly bedded	Well developed trough-cross stratification. Convolute bedding, slumping structures and asymmetric current ripples	Ribbons up to 18.5 m thick	Petrified wood fragments	Erosionally based. Common rip-up clasts up to 8.1 cm in length. Fining-upward trends	FA1A: trunk river channel FA1B: crevasse feeder channels
2	Siltstone, sandstone, carbonaceous mudstone and coaly mudstone	Planar bedding and ripple lamination	Wedges and lobes proximal-distal to FA1	Abundant leaf imprints of Angaran flora (eg. *Cordaites Sulcivius, Lepidophyte, Cicadocea* (*Guramsania hosbairica*) and *Secrospiroxylon tolgoyensis*	Sharp planar contacts	Overbank - floodbasin
3	Off-white Si-rich mudstone with common fine-grained pyrite	Rhythmically, varve-like, planar lamination	Laterally extensive sheet up to c. 50 m thick and +20 km along strike	None observed	Well preserved along southern sub-basinal flank	Lacustrine
4	Predominantly bright and dull gassy coal interlaminated to interbedded with carbonaceous mudstone and coaly mudstone	Parallel lamination and very thin bedding	Laterally continous sheets up to 51m thick and extending min. 19.4km along strike		Sharp planar lower bounding surfaces. Upper contact erosional in places	Low-lying peat-mire ecosystem
5	Tidal rhytmites. Interbedded to interlaminated fine-medium grained sandstone, siltstone and mudstone. Common pyrite	Small scale herringbone cross-stratification, lensen, wavy, flaser and disturbed bedding. Horizontal and ripple lamination	Sheets up to c. 5m thick	Ichno fossils such as *Planolites* and *Skolithos* isp. in places. Rare *Conulariida* preserved near base of coal measures	Sharp planar contacts	Foreshore
6	Predominantly well-sorted fine to coarse-grained sandstone with subordinate siltstone and carbonaceous mudstone	Well developed trough-cross stratification, planar bedding and rare hummocky cross-stratification	Sandstone-dominated depositional wedge	Moderate presence of ichno fossils such as *Planolites* and *Skolithos* isp. in places	Transgressive surfaces of erosion (TSE) well developed	Shoreface

multistory sheet-like sandstone bodies up to 18.5 m thick. The basal bounding surfaces are sharp, irregular and erosional, often marked by bedload conglomerate deposits. Internally it is medium-thickly bedded with predominant TCS. Fossil wood fragments up to 34 cm in length are common in places. FA1a is well exposed as laterally continuous strike ridges along the northern flank of the sub-basin (Fig. 9). Vertically, the sandstone units vary in thickness as they pinch and swell at right angles to the axial unidirectional paleo-flow direction (Fig. 8E). Sub-facies FA1b comprises ribbon sandstone bodies, with a thickness of a c. 1-4 m. A thin ribbon-shaped sandstone unit with a width/thickness ratio of 8 was documented in the western part of the study area. FA1b sandstone bodies are erosional based single and vertically stacked units of pebbly fine- to medium-grained sandstone. FA1b are generally medium bedded and dominated internally by TCS with moderate set heights (Fig. 9C). FA1b are well exposed in the western part of the sub-basin, where Johnson et al. (2007) noted common convolute bedding, slumping, asymmetric current ripples and upward-fining trends.

Interpretation. Sub-facies FA1a is interpreted as the active fills of rapidly aggrading, multi-story, fault-bounded channel belts. This interpretation is based on architecture, common rip-up clasts, petrified wood fragments and sedimentary structures. Sub-facies FA1b is considered to represent sand-filled crevasse-splay feeder channels with low width/thickness ratios, branching of an entrenched, fault-bounded, axial (i.e. westward draining) trunk river system, developed along the northern flank of the sub-basin (Fig. 9E). Michaelsen et al. (2000) documented similar crevasse-splay feeder channels from the Late Permian Rangal Coal Measures in NE Australia. More recently, Wang et al. (2022) documented similar "pipelines" from the Eocene Willwood Formation, Bighorn Basin, USA. The presence of a partly preserved petrified tree trunk in upright growth position within FA2 deposits suggests a flashy fluvial run-off regime, possibly controlled by A) syn-tectonics or B) non-perennial drainage, or both.

Facies association 2 (FA2): Overbank

FA2 is characterized by inter-bedded fine to medium-grained light-medium grey sandstone, medium-dark grey siltstone and carbonaceous mudstone. Sedimentary structures are dominated by horizontal, graded and indistinct bedding and horizontal and ripple lamination, with occasional convolute bedding. Petrified wood and well-preserved plant material (Fig. 9B) are common to abundant, including macroflora such as *Cordaites Sulcivius, Lepidophyte, Cicadocea (Guramsania hosbairica)* and *Secrospiroxylon tolgoyensis* as previously reported by Orolmaa et al. 1999 and Johnson et al. 2007, among others. Results from field work show that strap-shaped carbon-coated leaf impressions of *Cordaites* are by far the predominant macroflora (Fig. 9B) and often occur as seasonal leaf litter. Siderite horizons, typically c. 25-70 cm thick, are common throughout FA2 (Fig. 10).

Interpretation. FA 2 is interpreted as proximal-distal overbank and flood basin deposits, based on its overall fine grain-size, sedimentary structures and common - abundant plant fossils. Johnson et al. (2007) noted the siderite indicate swampy, reducing conditions. Tang et al. (2023) reported similar siderite in the coal-bearing beds of the Late Permian Xuanwei Formation in Eastern Yunnan, China. The comprehensive study revealed four distinct forms of siderite deposits: A) stratiform-laminated, B) lens-like nodule, C) sandstone cementation, and D) fracture filling. At Tsagaan Tolgoi the siderite appears to occur primarily as sandstone cementation which Tang et al. (2023) interpreted as forming through cementation and precipitation within the intergranular pores of debris particles under reducing conditions.

Facies association 3 (FA3): Lacustrine

FA 3 is characterized by very well sorted, thinly laminated whitish quartz-rich claystone (Fig. 4). FA3 is best developed in the southwestern part of the sub-basin where it is up to c. 50 m thick. The prominent Tsagaan Tolgoi hill provides excellent exposures of FA3. There FA3 is characterized by thin horizontal varve-like laminae (Fig. 4B).

Interpretation. FA3 is interpreted based on its fine grain-size attributes, blanketing nature, and varve-like laminae to represent deposition in a relatively shallow lake. Given the substantial thickness and uniform nature, subsidence and sediment flux must have been constant over a

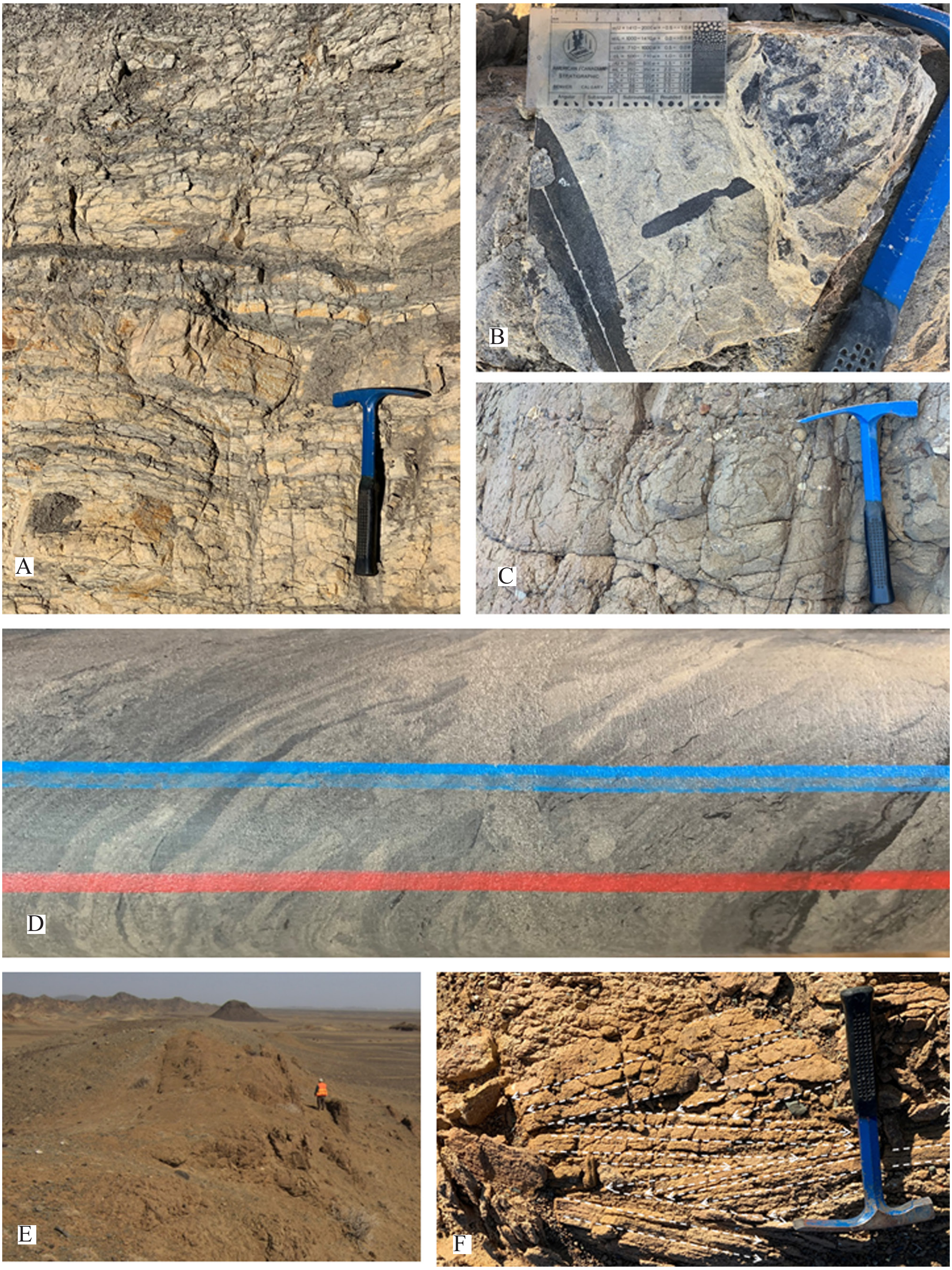

Fig. 9. Outcrop and drill core examples of facies association characteristics: A) Foreshore deposits of FA5, B) well preserved macroflora from FA2 overbank deposits, C) pebbly sandstone channel outcrop (FA1b) with well-developed TCS, D) FA5 deposits with disturbed bedding and ichno fossils, E) well developed active channel fill (FA1a) from the northern fault-bounded flank of the sub-basin, and F) HCS structures from bidirectional flow (FA5)

Fig. 10. A) Outcrop example of common shoreface deposits onlapping coal seams with transgressive surface of erosion B) Example of common siderite beds from seam 2 horizon, and C) classical shoaling-upward sequence showing low-angle hummocky cross-stratification developed above high-angle TCS

prolonged period. The lack of cross-lamination or rippled bedforms implies uniform low-energy conditions and minimal bottom-current activity. The rare occurrence of organic material indicates that water was sufficiently deep, and possibly anoxic, to preclude standing vegetation. The Tiaohu Formation of the Santanghu Basin in NW China, features thick successions of Permian tuffs formed in a deep lacustrine environment. Ma et al. (2016) reported that continuous volcanic ash settling periodically suffocated aquatic ecosystems. Further afield in the Cenozoic coal-bearing basins of Indonesia, the base sequence commonly comprises thick lacustrine shale -such as the "Brown Shale" or Pematang Group (Longley et al., 1990).

Facies association 4 (FA4): Peat mire

FA4 is composed of black coal, classified as high volatile B and C of the bituminous class and subbituminous A based on the internationally recognized ASTM D388 standard. FA4 is very well developed within the study area with a total of eight seam horizons (Fig. 5) and individual seams up to 50 m in apparent thickness. FA4 commonly contains numerous fine-grained clastic partings of FA2. The economically important seam horizon 1 is generally made up of a thick lower and upper seam couplet which coalesces over a strike length of c. 650 m proximal to the western sidewall fault to form a c. 50 m thick super seam. This thick basal seam 1 was intersected by Elixir Energy's Nomgon-1 CBM discovery well (Fig. 3). A very rare 34 cm thick pale brown tuff was noted in the basal part of seam 1, characterized by a low gamma ray response. Mapping work uncovered the thick basal seam 19.4 km east of Nomgon-1 along the southern flank of the sub-basin. Historical coal quality data from the western sector of the sub-basin indicates the thick basal seam would generally produce a raw low moisture, medium-high ash, moderate Sulphur and moderate energy product (Appendix Table 2, Fig. 11). Limited historical vitrinite reflectance

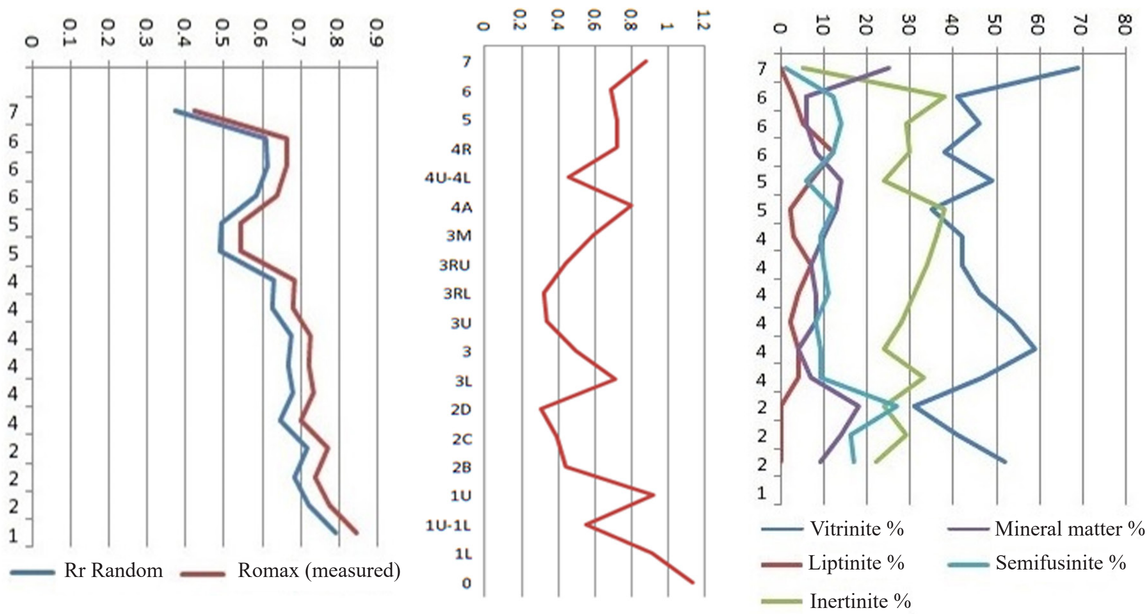

Fig. 11. A) Coal rank data showing an upward decrease in coal rank, B) Sulphur content of the eight coal seam horizons indicating an overall 3rd order sea-level cycle with superimposed 5th order cyclothems, and C) preliminary results from maceral analysis of the coal succession

(Ro) data from seam 1U-1L shows a value of 0.74. Independent vitrinite reflectance analysis from this study returned similar values of 0.776 (Appendix Table 3, Fig. 11A). All the coal seams at Tsagaan Tolgoi vary greatly in thickness and quality as shown in Appendix Table 2. The topmost Vitrinite-rich seam horizon 7 underlies the Permo-Triassic transitional boundary zone (Fig. 7). The thickness varies significantly from 2.1 - 13.3 m, with an average of 7.9 m. Coal quality data shows a relatively low ash average of 13.53% (dry basis), and it is noted that this is the lowest mean ash content of all the eight coal seams. Residual moisture average 5.52% (air dry basis), volatile matter average 35.07% (dry ash free basis), Sulphur of seam 7 varies significantly from 0.32-2.91% (dry basis) with an elevated average of 0.88% (Fig. 11B). The average gross calorific value for the topmost seam is 30.45 MJ (dry ash free basis). Ultimate analysis shows the highest Carbon values of the eight seams at 74.24% (Appendix Table 2). Significantly, ash composition testing from this study shows Sulphur trioxide values are the highest in the entire seam package with 6.88% compared to an average of 2.88% (Fig. 12). Further, ash composition testing shows that Mn_2O_3 is three times higher at 0.22% than the average of the seam package of 0.07%, and Fe_2O_3 are also elevated at 13.12% compared to 5.46% for the seam series (Fig. 12, Appendix Table 3). SiO_2 is lower at 50.94% than the average of 64.22% for the entire seam package and represents the culmination of an overall decreasing upward trend (Fig. 12). Furthermore, average K_2O values of 0.13% are almost five times lower than the average of 0.62% for the entire seam package (Fig. 12).

Interpretation. FA4 is considered to represent laterally extensive, low-lying peat mire systems developed on the lower coastal plain. In a sequence stratigraphic context, the facies stacking pattern suggest they primarily developed during transgressive systems tracts and early high-stand systems tracts times (Diessel, 1992, 2007; Shao et al., 2003). During transgressive systems tracts times the sea slowly advances with the coastal areas experience a rising water table which allows peat-forming ecosystems to spread and keep pace with the rising water level, whereas during early highstand systems tracts times the sea-level rise slows down and coal-forming plants can accumulate in a high-water table environment (Diesel, 2007). Basal seam 1 probably represents a prolonged period of deposition given the significant thickness. The relatively thick (av. 7.85 m) topmost seam 7 is relatively low in ash (13.53% dry basis) and high in vitrinite (69%). In this context Diessel (2007) noted that simple properties, such as maximum coal thickness, low detrital mineral content and

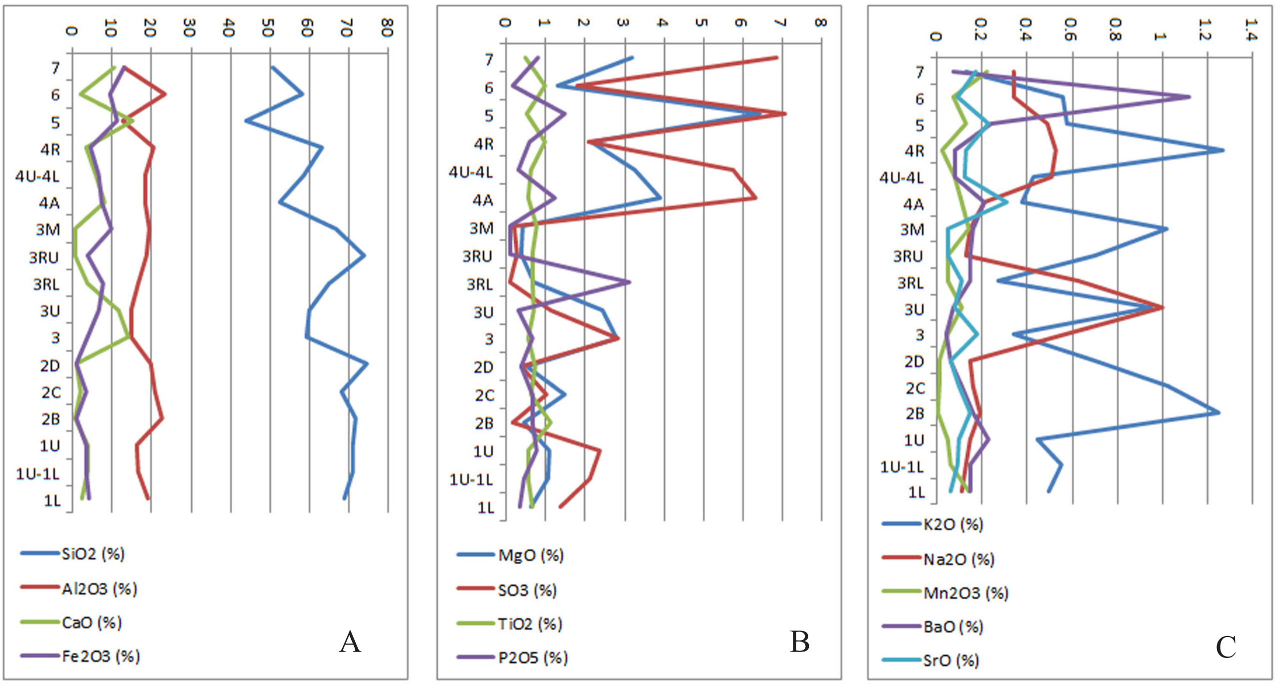

Fig. 12. Ash composition elements of the Late Permian coal horizons (text for discussion)

maximum preservation of vitrinite, define a good balance between accommodation versus peat accumulation, as such, Seam 7 probably accumulated during transgressive to early highstand systems tracts times of the final high frequency sea-level rise prior to the deep End Permian lowstand.

Facies association 5 (FA5): Foreshore

FA5 is characterized by inter-bedded to inter-laminated fine to coarse-grained sandstone, medium-dark gray siltstone and carbonaceous mudstone with common pyrite. These sediments are moderately bioturbated (Fig. 9D) and contain disintegrated organic material in places. Depositional structures include small scale herringbone cross-stratification (HCS), tidal bundles, wavy, disturbed, lenticular and parallel bedding. The preserved set heights of the rare HCS vary from 7.5 - 11.3 cm, whereas the grain size is coarse-very coarse-grained sandstone (Fig. 9F). The level of bioturbation intensity within FA5 is generally moderate, however, varying significantly from Bioturbation Index 0 to 4 in the scheme of Bann and Fielding, 2004. The biogenic structures are characterized by a low diversity assemblage of sand-filled *Planolites* and inclined structures (Fig. 9D). A fragment of a very rare *Conulariida* (ie. an extinct group of medusozoan cnidarians) was discovered within carbonaceous mudstone deposits of FA5 within the basal part of the formation (Fig. 6).

Interpretation. FA5 is interpreted as inter-tidal flat deposits developed along the foreshore of a mesotidal depositional environment based on sedimentary structures and overall moderate presence of ichnofossils. The diagnostic HCS structures were discovered at 42°52’32.64”N/105°27’45.56”E (Fig. 6) proximal to the Nomgon-1 CBM discovery well. HCS is widely used as a proxy to identify ancient tidally dominated environments (Eriksson, 1977; Singh, 1980; Daidu et al., 2013). HCS in very coarse to coarse-grained sandstone beds forms in high-energy, tidally influenced environments where alternating water currents (flood and ebb tides) migrate back and forth (Reading, 1996). The HCS sedimentary structures probably developed during symmetrical tidal dynamics where flood and ebb currents were both sufficient to carry the coarse-grained sediments. Similar inter-tidal deposits were documented within the Late Permian coal measures at Bayanjargalant in central Mongolia by Michaelsen (2016) and Michaelsen and Demberelsuren (2024). The very rare *Conulariida* fragment discovered at 42°53’39.26”N/105°32’48.83”E c. 50 m south of the Carboniferous basement contact, was emplaced during a brief shallow marine incursion. The *conulariida* fragment measured 10mm in length, showing 12-13 transverse ribs (Fig. 6). The fragmented preservation of the *conulariia* fragment on the foreshore might signify a relatively high-energy depositional environment where the holdfast was dislodged and the animal disjointed during a storm event. Significantly, Michaelsen (2016) reported a similar very rare *Conulariida* fragment from the base of the Late Permian coal measures at Bayanjargalant 524 km to the northeast.

FA6: Shore face

FA6 is characterized by light-medium gray, well sorted, very fine-coarse grained sandstone, interbedded with subordinate medium-dark gray siltstone and dark gray to blackish mudstone. FA6 is very well represented in the lower part of the sedimentary package, particularly between seam horizons 2 and 3 and seam horizons 3 and 4. Sedimentary structures include rare low amplitude hummocky cross stratification (Fig. 9F), well developed TCS with set height up to 93.2 cm, planar and disturbed bedding. FA6 commonly overlies FA4 (example show in Fig 10A). Ichnofossils such as *Skolithos* and *Planolites* isp. (Fig. 9D, Pemberton and Frey, 1982; Bromley, 1996) were documented during field work. The level of bioturbation intensity is low, generally ranging from 0 to 1. Rudimentary microscopic analysis of the sandstone composition shows well sorted, fine-medium grained, texturally immature sandstone, with dominantly angular to sub-angular grains often characterized by very low sphericity. Framework grains are dominated by labile volcano-lithics, limited feldspars and c. 20% quartz grains. Clearly, the framework grains were not significantly upgraded in the shallow marine realm (Michaelsen and Henderson, 2000), suggesting rapid deposition and burial.

Interpretation. FA6 is interpreted as shallow marine (shore face) deposits based on diagnostic sedimentary structures and lithological composition. The rare low-angle amplitude hummocky cross stratification structures overlie well sorted medium-grained sandstone with TCS with set height measured at 40-50 cm (Fig.

Fig. 13. A) Rare example from the middle part of the Late Permian coal measures of large, petrified tree trunk in growth position, indicating rapid clastic aggradation at times. The tree trunk was measured at +116.4 cm in length and 44.2 cm in width, B) Example of thick well-developed growth rings from the lower part of the YUF (i.e. coal seam 3 horizon), and C) Petrified wood trunk from coal seam 4 horizon

Table 3. Preliminary results from rudimentary growth ring analysis (text for discussion)

Specimen # / In-situ measurement	Stratigraphic position	Specimen width (cm)	Total # of rings	Maximum width (mm)	Minimum width (mm)	Mean width (mm)
TTS7001	Above Seam 7	4.9	14	12	1	3.57
TTS7002	Above Seam 7	7.2	13	7	3	5.08
TTS7003	Above Seam 7	8.1	15	9	2	4.53
TTS7004	Above Seam 7	4.8	10	9	2	3.36
TTS7005	Above Seam 7	11.2	24	11	2	3.92
TTS7006	Above Seam 7	13.5	21	10	1	4.24
In-situ	Seam 4 horizon	18.3	42	7	1	3.98
In-situ	Seam 3 horizon	28.4	20	19	9	12.55

9F). This vertical sequence is a classic indicator of a regressive (shoaling-upward) sedimentary environment, reflecting a transition from a deeper to shallower storm-influenced setting, generated by: A) a prograding coastline, or alternatively B) a marine regression. Hummocky cross stratification represents shallower water depths between the fair-weather wave base and storm wave base with a depth ranging significantly from c. 2 to +80 m (Dott and Bourgeois, 1982). They are created by the intense, chaotic orbital motion of water combined with bottom-hugging currents during severe storm events as documented by Dott and Bourgeois (1982). In essence, the discovery of amplitude hummocky cross stratification structures indicates a high energy depositional environment.

Depositional environments

The sandstone-to-mudstone ratio was estimated for the lower part of the coal measures (i.e. seam horizons 0-4) at 1.87 based on analysis of the deep Nomgon-1 CBM discovery well. The ratio is considered to represent an overall moderate to relatively high energy setting (Reading, 1996). This quantitative data supplements the work by Johnson et al. (2007) on the mudstone-dominated upper section, showing an overall upward-fining and reduced energy shift (Fig. 4). The facies analysis of this study shows the YUF developed in a dynamic transitional depositional environment proximal to the paleo shoreline, characterized by frequent transgressive-regressive cycles marked by the inter-digitation of paralic-shallow marine and alluvial strata. The abrupt facies changes (Fig. 10A) documented here could be a product of syn-tectonic controlled fluctuations in accommodation-to-sediment supply (Gardner et al., 2004). High frequency Milankovitch-type cyclothems are evident within the coal measures from facies stacking patterns, diagnostic sedimentary structures such as herringbone- and hummocky cross-stratification and coal-chemical signatures. The facies analysis indicates a mesotidal depositional environment based on diagnostic sedimentary structures such as HCS and lenticular bedding and the moderate presence of ichno fossils (Table 2). The occurrence of hummocky cross stratification within FA6 deposits (Fig. 10C) strongly indicates a high energy shallow marine environment, flanked by a c. 20-300 m wide foreshore (Anfuso and Ruiz, 2004). The precise width of the foreshore is dictated by the slope of the beach. The common abrupt superposition of shallow marine FA6 sandstone beds immediately above coal seams (Fig. 10A) was observed above seven coal seams in the Nomgon-1 core and might be a result of rapid syn-tectonic generated accommodation space caused by reactivation of growth faults (Fig. 3). The immature textural and compositional nature of sandstone framework grains suggest overall rapid aggradation, interrupted by deposition of thick blanketing peat-mires during transgressive to early high-stand systems tracts times (Diessel, 1992, 2007; Chou, 2012). The punctuated aggradation interpretation is supported by the discovery of a +1.16 m long, and 44.2 cm wide petrified tree trunk partially preserved in upright growth position perpendicular to strike (Fig. 13). Climatic indicators within the Late Permian coal measures include well developed annual growth rings in petrified wood trunks measuring up to 52.1 cm across and up to 9.5 m in length (Fig. 13B-C). Detailed growth ring analysis on fossilized wood obtained from the YUF by Cai

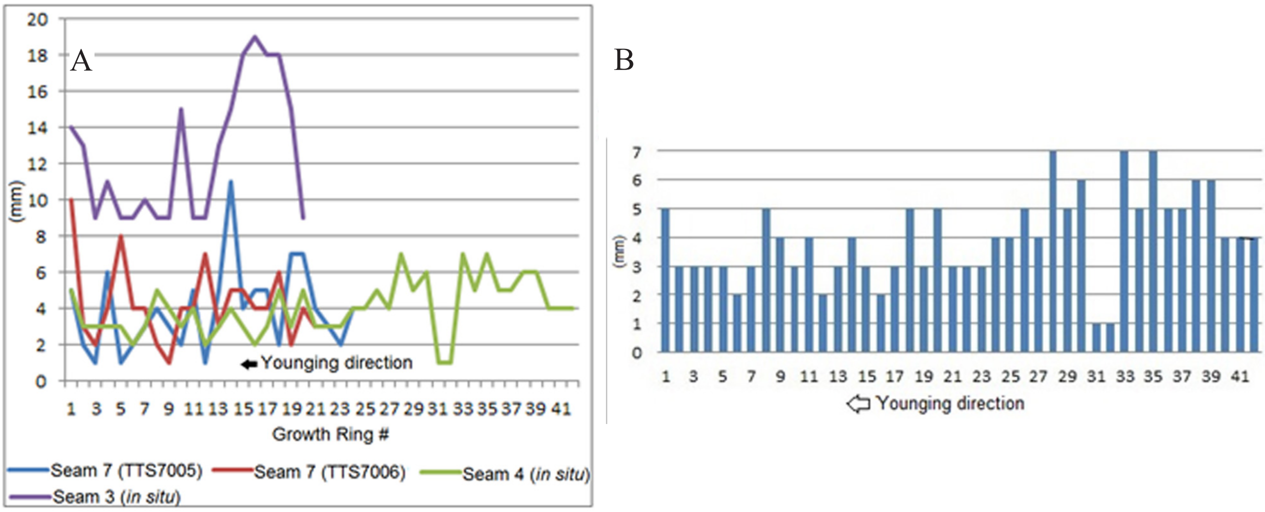

Fig. 14. Preliminary results from rudimentary fossil wood growth ring analysis from coal seam horizons 3, 4 and 7 indicating climatic instability and deteriorating conditions towards the PTB, and B) fossil wood growth ring analysis from coal seam 4 horizon (text for discussion)

et al. (2023), suggested relatively short growing seasons. Further, the authors discovered a growth interruption, probably recording an early spring cooling event in a temperate climate. Cai et al. (2023) noted that growth rings are inconspicuously present in the studied stem, whereas false rings are commonly present throughout the secondary xylem, indicating eco-physiological anatomical responses to continuous environmental turbulence under indistinctive seasonal climatic conditions during the latest Permian. The detailed work by Cai et al. suggests that while the End-Permian was globally characterized by a significant warming trend of 10°C towards the EPME (Ragon et al., 2025), the Yamaan Us peat mire ecosystem might have experienced a short-lived cooling event during overall increasingly warmer conditions. This is supported by the presence of the *Conulariida* (Fig. 6) which preferred cooler Permian waters (Waterhouse, 1979). Further, recent work by Fielding et al. (2022, 2023) on Late Permian strata in NE Australia showed that cold climate persisted until 253 Ma. Rudimentary growth rings analysis on a total of eight petrified trunk samples from coal horizons 3, 4 and 7 were recently conducted (Table 3, Fig. 14). Preliminary results from the limited samples indicates: 1) significant variation in annual growth ring width in every analyzed sample (examples shown in Fig. 14); 2) ring width averaged 4.12 mm for seam horizon 7, 3.98 mm for seam horizon 4 and 12.55 mm for seam horizon 3; 3) a marked decrease in growth ring thickness upwards from seam horizon 3 towards the PTB, and 4) ring structures for the petrified wood associated with horizons 3 and 4 coals are similar being strongly dominated by earlywood, whereas the six samples obtained above the topmost Seam 7 are still dominated by earlywood cells but all have thicker latewood cell ratio than the stratigraphically underlying samples. The significant variations in annual growth rings indicate environmental stress (i.e. potential pulses of toxic gas exhalation from the contemporary Siberian Traps coupled with variations in sunlight, precipitation and overall increasing temperature). These preliminary results are in line with the findings of the detailed study by Cai et al. (2023) which indicated continuous environmental turbulence during the latest Permian.

Frequent wildfires during the Late Permian have recently been reported from numerous global studies (Bhattacharya et al., 2025; Hua et al., 2024; Jiao et al., 2023; Mays and Mcloughlin, 2022; Song et al., 2022; Lu et al., 2022; Cai et al., 2021; Vajda et al., 2020; Jasper et al., 2016), and commonly associated with elevated levels of inertinite (charcoal). Mays and Mcloughlin (2022) quantitatively demonstrated a clear spike in wildfire activity around the EPME. Fire-scarred petrified wood are extremely rare in Late Permian outcrops in Mongolia. Thus far only a few fire-scarred fragments have been discovered (i.e. all above the topmost seam 7 at Tsagaan Tolgoi). These very rare samples resemble the ones reported by Byers et al. (2020) and interpreted here as being caused by outgassed methane ignited by lightning. Preliminary maceral data from the YUF are presented in Appendix Table 3 and summarized in Fig. 11C. Of the three primary groups vitrinite dominate with 31-69% and average 46%. The inertinite group varies from 5-38% and average 28% - generally increasing upwards, however, with very low values of 5% in the topmost seam. Liptinite varies significantly from 1-27 %, av. 12%, and mineral matter varies from 6-25% with 10% av. Historical vitrinite reflectance measurements (ie. RoMax) for seams 1U-1L, 4U-4L and 4R indicate a thermal maturity range of 0.74-0.63, mirroring the results of this study (Appendix Table 4). Further, the historical thermal maturity range of 0.74-0.63 implies a maximum burial depth of 2 km (Underdown et al., 2007). The RoMax results of this study are up to 0.847 indicating a maximum burial depth of c. 2.5-3.5 km. This, in turn, indicates that the Triassic deposits were originally much thicker, with significant erosion during inversion.

DISCUSSION

Deposition of the c. 550 m thick Late Permian coal measures in the TTSB came to a halt after the deposition of the up to 13.3 m thick topmost coal seam 7. It is noted that while the lithostratigraphic record shows no general diminution in the thickness or spatial distribution of coal seams prior to the EPME, other data such as fossil wood growth ring analysis by Cai et al. (2023) coupled with the preliminary results from this study (Table 3), indicate continuous environmental turbulence during the latest Permian. In this context, recent work by Fielding et al. (2022) in Australia concluded that the Late Permian fossil floras indicate remarkably consistent terrestrial ecosystems throughout the late Lopingian right until the EPME. The isotope study and palynological record across the PTB at TTSB by Johnson et al. (2007), complimented by the facies analysis from this study, provides an important record of very significant climatic and environmental changes at a critical period of Earth history. In general, the palynological and sedimentological record shows an abrupt aridification transition, probably driven by rapid, volcanically degassing induced greenhouse warming (Nagy et al., 2026). The transition is characterized by a significant change from humid fluvial to paralic coal-forming environments during the Late Permian to arid desolate terrestrial conditions during Early Triassic times, accompanied by a deep regression across the PTB (Hallam, 1992). Recent work across the PTB in the Sydney Basin, Australia, by Vajda et al. (2020) found recovery of vascular plants evident <2 m above the EPME level. Further, new research from North China by Guo et al. (2026) documented rapid riparian ecosystem recovery following the end-Permian mass extinction. However, thus far no evidence of Early Triassic macro flora or ichno fossils has been uncovered from the Early Triassic succession within the TTSB. Johnson et al. (2007) reported *Taeniate*-striate *bisaccate* pollen within the lowermost Triassic sediments, which is typically associated with evaporites and arid conditions. While no evaporates were observed during field work, barren arid conditions were confirmed, with common pedogenic carbonate nodules (Fig. 8C) suggesting an arid to semi-arid region where evaporation outpaced rainfall (Gocke et al., 2012).

At the PTB pulses of volcanic gas release from the Siberian Traps undoubtedly released catastrophic amounts of sulphur gases into the atmosphere (Augland et al. 2019; Shen et al., 2018; Dal Corso et al., 2022). These gases rapidly oxidize into sulphuric acid and sulphur trioxide creating widespread acid rain, and environmental toxicity. It is therefore likely that gases from the Great Siberian Trap volcanism led to environmental consequences of unknown extent, but with obvious impact in northwestern Siberia and parts of Central Asia. However, in a global and geohistorical context, this was probably only a large regional event superimposed on a general global outgassing - both through the seafloor and on land. This is the basis of the degassing-related dynamo-tectonic theory - Global Wrench Tectonics, on which the interpretation of the formation and development of the Tsagaan Tolgoi basin with TTSB. The degassing-related development of the Earth's crust has been stepwise, as expressed in the geological time scale. There is a close correlation between changes in the Earth's moment of inertia (with associated changes in the Earth's rotation), the surface tectonic pattern, the pulse-like supply of seawater from the interior, oceanization (delamination) of the originally pan-global continental crust, the transport and unloading mechanisms of metals by ascending gases and fluids, air and ocean pollution, and biological disasters. This leads to a coherent multi-phenomenological Earth history in which the most striking biological extinctions are closely linked to the major geological time boundaries which are also linked to marked sea level regressions. It is therefore very likely that the Earth's degassing-related modus operandi, with a factual basis hidden in an enormous number of published works, must form the theoretical platform for any realistic interpretation of problems of a geological or environmental nature. In an evolving physical system, such as the Earth, all surface end products will form a naturally coherent phenomenological network. The ultimate purpose of any science is, then, to be able to recognize this physical pattern in a jumble of individual observations - and thus establish a working paradigmatic foundation.

Dal Corso et al. (2024) documented repeated pulses of sulphur-rich volcanic gases that had driven the biological and environmental crisis in Northwest China at the end of the Permian, but volcanism itself is also a product of Earth's degassing (Hunt et al., 1992). At Tsagaan Tolgoi the topmost seam 7 which underlies the PTB is characterized by the highest concentration of Sulphur trioxide of 6.88% (compared to an average of 2.88% for the entire seam package. The relationship between total sulphur in coal and sea-level changes is well established (Diessel, 1992, 2007; Chou, 2012). Combining the Sulphur curve for the Tsagaan Tolgoi seam package (Fig. 7B) with the results from the facies analysis of this study, suggest the coal measures developed during a single 3rd order sea-level cycle (Fig. 7B), with superimposed 5th order para-sequences (Van Wagoner et al., 1990). Such cycles are well established within Permian strata on a global scale (Lanci et al., 2022). The duration of the 3rd order cycle was previously estimated at 0.5-5 My by Haq et al. (1988), but recently significantly revised to c. 0.5-2.5 My by Haq and Ogg (2024) with 5th order cycles averaging 100 Ky. It is highlighted here that: 1) geometrically, individual 3rd order cycles are characterized by asymmetry, with overall slow transgression followed by rapid regression, and 2) temporally, the stacking pattern of these cycles are also strongly asymmetrical as the revised charts by Haq and Ogg (2024) illustrates. In turn, these repeated patterns strongly argue for intermittent tectonic pulses on a global scale driven by subcrustal forces (Umbgrove, 1942/1947) - such as those that build up and are released in a degassing Earth.

SUMMARY

-In the TTSB, a total of six recurrent coal-bearing facies associations, from fluvial to shallow marine, have been defined. The architectural and temporal relationships allow a preliminary reconstruction of the syn-tectonic coal-bearing system.

-A mesotidal depositional setting is strongly suggested by sedimentary structures such as lenticular bedding, HCS and the moderate presence of ichno-fossils. High energy shoreface deposits are well preserved with diagnostic hummocky cross-stratification

-Dramatic aridification is recorded across the PTB, from humid coal forming to desolate arid conditions, based on palynology and the sedimentary record.

-The sedimentary record coupled with available coal quality and petrographic data suggest the Late Permian Yamaan Us coal measures developed during a single 3rd order sea-level cycle with duration of c. 0.5-2.5 My. Primary control of the stratigraphic architecture refers to upper crustal wrench tectonics, possibly with superimposed high-frequency orbital Milankovitch cycles.

-The main mechanism behind the development of the Tsagaan Tolgoi basin with TTSB, as well as all other dynamo-tectonic processes affecting the Earth, is the planet's ongoing degassing towards thermochemical equilibrium. In this context, the development of the basin becomes a snapshot of billions of years of outgassing that has given rise to all aspects of the Earth's internal constitution, crustal tectonic history, and surface products.

ACKNOWLEDGEMENTS

The authors thank two anonymous reviewers for their constructive comments and suggestions, which greatly improved the quality of the manuscript. The following are thanked for their assistance with identifying flora and fauna: Professor Vietor Ogar, Kyiv National University, Dr. Vitaliy Dernov, National Academy of Sciences of Ukraine, Professor Heyo Van Iten, Hanover College, Dr. Eduard Mychko, Russian Academy of Sciences and Dr. Spencer Lucas, New Mexico Museum of Natural History and Science. Dr. Demberelsuren Batbold, Energy Resources Mongolia, is greatly acknowledged for processing and analyzing the coal quality samples.

Authorship

Conceptualization and project administration: both authors; field work: Per Michaelsen; conceptualization of wrench tectonics and degassing model: Karsten M. Storetvedt; methodology and depositional model: Per Michaelsen; writing original draft, review and editing: both authors.

Conflict of Interest

The authors declare no conflict of interests.

REFERENCES

Anfuso, G. Ruiz, N. 2004. Morphodynamics of a mesotidal, exposed, low tide terrace beach (Faro, southern Portugal). Ciencias Marinas, vol. 30(4), p. 575-584. https://doi.org/10.7773/cm.v30i4.341

Aristov, D.S. 2005. New Grylloblattids (Insecta: Gryllobattida) from the Triassic of Eastern Europe, Eastern Kazakstan, and Mongolia. Paleontological Journal, vol. 39(2), p. 173-177.

Augland, L.E., Ryabov, V.V., Vernikovsky, V.A., Planke, S., Polozov, A.G., Callegaro, S., Jerram D.A., Svensen, H.H. 2019. The main pulse of the Siberian Traps expanded in size and composition. Scientific Reports, vol. 9, 18723 https://doi.org/10.1038/s41598-019-54023-2

Austrheim, H. 1987. Eclogitization of lower crustal granulites by fluid migration through shear zones. Earth and Planetary Science Letters, vol. 81(1-3), p. 221-232. https://doi.org/10.1016/0012-821X(87)90158-0

Bann, K.L., Fielding, C.R. 2004. An integrated ichnological and sedimentological comparison of non-deltaic shoreface and subaqueous delta deposits in Permian reservoir units of Australia. Geological Society, London, Special Publications, vol. 228(1), p. 273-310. https://doi.org/10.1144/GSL.SP.2004.228.01.13

Bhattacharya, S., Summons, R.E., Murthy, S., Foster, C., Husain, F., Ankit, Y. 2025. Impact of wildfires on Gondwanan flora during the Permian-Triassic transition. Geochemical Perspectives Letters, vol. 36, p. 35-41. https://doi.org/10.7185/geochemlet.2532

Bromley, R.G. 1996. Trace Fossils. Biology, Taphonomy and Applications, 2nd ed. 361 pp. Chapman & Hall, London, 361 p.

Burenkhuu, E., Gotovsuren, A., Badarch, G., Dagvatseren, A. 1995. Report of geological complex study of the Galviin Gobi area (1987-1989) at scale 1:200,000. Ulaanbaatar, National Geological Survey, no. 4877.

Byers, B.A., DeSoto, L., Chaney, D., Ash, S.R., Byers, A.B., Byers, J.B., Stoffel, M. 2020. Fire-scarred fossil tree from the Late Triassic shows a pre-fire drought signal. Scientific Reports, vol. 10, 20104. https://doi.org/10.1038/s41598-020-77018-w

Cai, Y.F., Zhang, H., Biao P. 2024. Charcoal evidence traces diverse fungal metabolic strategies to the Late Paleozoic. iScience, vol. 27(6), 110000. https://doi.org/10.1016/j.isci.2024.110000

Cai, Y.F., Zhang, H., Feng, Z., Gou, X.D., Byambajav, U. Zhang, Y.C., Yuan, D.X., Qie, W.K., Xu, H.P., Cao, C.Q., Yarinphil, A., Shen, S.Z. 2022. A new conifer stem, *Ductoagathoxylon tsaaganensis*, from the Upper Permian of the South Gobi Basin, Mongolia and its palaeoclimatic and palaeoecological implications. Review of Palaeobotany and Palynology, vol. 304, 104719. https://doi.org/10.1016/j.revpalbo.2022.104719

Cai, Y.F., Zhang, H., Feng, Z., Zhang, Y.C., Yuan, D.X., Xu, H.P., Byambajav, U., Yarinphil, A., Shen, S.Z. 2023. *Secrospiroxylon tolgoyensis* gen. nov. et sp. nov., a unique coniferous stem from the uppermost Permian of the South

Gobi Basin, Mongolia, and its palaeoclimatic, palaeoecophysiological, and palaeoecological implications. Palaeontographica Abteilung B, vol. 305 (1-4), p. 93-119. https://doi.org/10.1127/palb/2023/0080

Cai, Y-F., Zhang, H., Cao, C-Q., Zheng, Q-F., Jin, C-F., Shen, S-Z. 2021. Wildfires and deforestation during the Permian-Triassic transition in the southern Junggar Basin, Northwest China. Earth-Science Reviews, vol. 218, 103670 https://doi.org/10.1016/j.earscirev.2021.103670

Channon, G., Young, N. 2019. Coal Bed Methane in the South Gobi Basin, Mongolia. Abstract in the Proceedings of the 2019 South East Asia Petroleum Exploration Society (SEAPEX) Conference, p. 53.

Chou, C-L. 2012. Sulfur in coals: A review of geochemistry and origins. International Journal of Coal Geology, vol. 100, p. 1-13. https://doi.org/10.1016/j.coal.2012.05.009

Collinson, J.D., Thompson. D.B. 1982. Sedimentary Structures. London, Allen and Unwin, 207 p.

Cui, Y., Li, M., van Soelen, E.E., Kürschner, W.M. 2021. Massive and rapid predominantly volcanic CO2 emission during the end-Permian mass extinction. PNAS, vol. 118(37), e2014701118. https://doi.org/10.1073/pnas.2014701118

Daidu, F., Yuan, W. Min, L. 2013. Classifications, sedimentary features and facies associations of tidal flats. Journal of Palaeogeography, vol. 2(1), p. 66-80. https://doi.org/10.3724/SP.J.1261.2013.00018

Dal Corso, J., Newton, R.J., Zerkle, A.L., Chu, D., Song, H., Song, H., Tian, L., Tong, J., Di Rocco, T., Claire, M.W., Mather, T.A., He, T., Gallagher, T., Shu, W., Wu, Y., Bottrell, S.H., Metcalfe, I., Cope, H.A., Novak, M., Jamieson, R.A., Wignall, P.B. 2024. Repeated pulses of volcanism drove the end-Permian terrestrial crisis in northwest China. Nature Communications, vol. 15, 7628. https://doi.org/10.1038/s41467-024-51671-5\

Dal Corso, J., Song, H., Callegaro, S., Chu, D., Sun, Y., Hilton, J., Grasby, S.E., Joachimski, M.M., Wignall, P.B. 2022. Environmental crises at the Permian-Triassic mass extinction. Nature Reviews Earth & Environment, vol. 3, p. 197-214. https://doi.org/10.1038/s43017-021-00259-4

Demberelsuren, B., Jargal, L., Munkhtsengel, B., Lkhagva-Ochir, S., Ganzorig, R., Tsolmon, A., Enkhbat, Ch., Turbat, E., Tuvshinbayar, E., Tugsjargal, A. 2023. Coal facies of the Middle Permian Baruunnaran deposit, South Mongolia. Mongolian Geoscientist, vol. 28 (57), p. 71-91. https://doi.org/10.5564/mgs.v28i57.3236

Diessel, C.F.K. 1992. Coal-Bearing Depositional Systems. Springer-Verlag, 721 p. https://doi.org/10.1007/978-3-642-75668-9

Diessel, C.F.K. 2007. Utility of coal petrology for sequence-stratigraphic analysis. International Journal of Coal Geology, vol. 70(1-3), p. 3-34. https://doi.org/10.1016/j.coal.2006.01.008

Dimitrov, L.I. 2002. Mud volcanoes - the most important pathway for degassing deeply buried sediments. Earth-Science Reviews, vol. 59(1-4), p. 49-76. https://doi.org/10.1016/S0012-8252(02)00069-7

Dott, R.H.Jr. Bourgeois, J. 1982. Hummocky cross-stratification: significance of its variable bedding sequences. GSA Bulletin, vol. 93(8): 663-680. https://doi.org/10.1130/0016-7606(1982)93<663:HSSOIV>2.0.CO;2

Durante, M.V. 1976. The Paleobotanical Basis for Stratigraphy of the Carboniferous and Permian of Mongolia. Proceedings of the Joint Soviet-Mongolian Geological Expedition, vol. 19, Moscow, Nauka, 304 p.

Durante, M.V., Luvsantseden, U. 2002. Developmental features of the southern branch of the Subangaran paleofloristic region. In: Akhmetiev, M.A., Herman, A.B., Doludenko, M.P., Ignatiev, I.A. (Eds.). Special volume, dedicated to the memory of the Corresponding member of the USSR Academy of Sciences, Professor Vsevolod Andreevich Vakhrameev (to the 90th anniversary of his birth). Geological Institute, Russian Academy of Sciences, Moscow, GEOS, p. 247-261.

Eriksson, K.A. 1977. Tidal deposits from the Archaean Moodies Group, Barberton Mountain Land, South Africa. Sedimentary Geology, vol. 18(1-3), p. 257-281. https://doi.org/10.1016/0037-0738(77)90015-X

Fielding, C.R., Frank, T.D., Birgenheier, L.P. 2023. A revised, late Palaeozoic glacial time-space framework for eastern Australia, and comparisons with other regions and events. Earth-Science Reviews, vol. 236, 104263. https://doi.org/10.1016/j.earscirev.2022.104263

Fielding, C.R., Frank, T.D., Savatic, K., Mays, C., McLoughlin, S., Vajda, V., Nicoll, R.S. 2022. Environmental change in the late Permian of Queensland, NE Australia: The warmup to the end-Permian Extinction. Palaeogeography, Palaeoclimatology, Palaeoecology, vol. 594, 110936. https://doi.org/10.1016/j.palaeo.2022.110936

Folk, R.L. 1974. Petrology of Sedimentary Rocks. Austin, Texas, Hemphill Publishing Company, 182 p.

Gardner, M.H., Cross, T.A. Levorsen, M. 2004. Stacking Patterns, Sediment Volume Partitioning, and Facies Differentiation in Shallow-Marine and Coastal-Plain Strata of the Cretaceous Ferron Sandstone, Utah. In: Chidsey, T.C.Jr., Adams, R.D. Morris, T.H. (Eds.) Regional to Wellbore Analog for Fluvial-Deltaic Reservoir Modeling: The Ferron Sandstone of Utah. https://doi.org/10.1306/St50983C5

Gocke, M., Pustovoytov, K. Kuzyakov, Y. 2012. Pedogenic carbonate formation: Recrystallization versus migration-Process rates and periods assessed by 14C labeling. Global Biogeochemical Cycles, vol. 26(1), GB1018. https://doi.org/10.1029/2010GB003871

Guo, W., Tian, L., Chu, D., Shu, W., Benton, M.J., Liu, J., Tong, J. 2026. Rapid riparian ecosystem recovery in low-latitudinal North China following the end-Permian mass extinction. eLife 14, RP104205. https://doi.org/10.7554/eLife.104205.4

Hallam, A. 1992. Phanerozoic Sea-Level Changes. New York, Columbia University Press, 265 p.

Haq, B., Hardenbol, J., Vail, P., Stover, L.E., Colin, J.P., Ioannides, N.S., Wright, R.C., Baum, G.R., Gombos, A.M., Pflum, C.E., Loutit, T.S., Jan du Chene, R., Romine, K.K., Sarg, J.F., Posamentier, H.W., Morgan, B.E. 1988. Mesozoic and Cenozoic chronostratigraphy and cycles of sea-level change. SEPM Special Publication 42, p. 71-108. https://doi.org/10.2110/pec.88.01.0071

Haq, B.U., Ogg, J.G. 2024, Retraversing the Highs and Lows of Cenozoic Sea Levels: GSA Today, vol. 34(6), p. 4-11. https://doi.org/10.1130/GSATGG593A.1

Hongfu, Y., Kexin, Z., Jinnan, T., Zunyi, Y., Shunbao, W. 2001. The Global Stratotype Section and Point (GSSP) of the Permo-Triassic boundary. Episodes, vol. 24(2), p. 102-114. https://doi.org/10.18814/epiiugs/2001/v24i2/004

Hovland, M., Fichler, C., Rueslatten, H., Johnsen, H.K. 2006. Deep-rooted piercement structures in deep sedimentary basins - Manifestations of supercritical water generation at depth? Journal of Geochemical Exploration, vol. 89(1-3), p. 157-160. https://doi.org/10.1016/j.gexplo.2005.11.056

Hua, F., Shao, L., Wang, X., Jones, T.P., Zhang, T., Bond, D.P.G., Yan, Z., Hilton, J. 2024. The impact of frequent wildfires during the Permian-Triassic transition: Floral change and terrestrial crisis in southwestern China. Palaeogeography, Palaeoclimatology, Palaeoecology, vol. 641, 112129. https://doi.org/10.1016/j.palaeo.2024.112129

Hunt, C.W., Collins, L.G., Skobelin, E.A. 1992. Expanding Geospheres: Energy and Mass Transfers from Earth's interior. Calgary, Polar Publishing, 421 p.

Ignatov, M.S. Shcherbakov, D.E. 2011. Lower Triassic mosses from Yamanus (Mongolia). Arctoa, vol. 20, p. 65-80. https://doi.org/10.15298/arctoa.20.04

ISO 7404-2, 2009. International Standard. Methods for the petrographic analysis of coals-Part 2: Methods of preparing coal samples. 12 p.

ISO 7404-3, 2009. International Standard. Methods for the petrographic analysis of coals-Part 3: Method of determining maceral group composition. 7 p.

ISO 7404-5, 2009. International Standard. Methods for the petrographic analysis of coals-Part 5: Method of determining microscopically the reflectance of vitrinite. 15 p.

Ito, T., Zoback, M.D. 2000. Fracture permeability and in situ stress at 7 km depth in the KTB scientific drillhole. Geophysical Research Letters, vol. 27(7), p. 1045-1048. https://doi.org/10.1029/1999GL011068

Jasper, A., Uhl, D., Agnihotri, D., Tewari,

Pandita, S.K., Benicio, J.R.W., Pires, E.F., Rosa, A.A.S.D., Bhat, G.D., Pillai, S.S.K. 2016. Evidence of wildfires in the Late Permian (Changsinghian) Zewan Formation of Kashmir, India. Current science, vol. 110(13). 419-423.
https://doi.org/10.18520/cs/v110/i3/419-423

Jiao, Sh, Zhang, H., Cai, Y., Chen, J., Feng, Z., Shen, S. 2023. Collapse of tropical rainforest ecosystems caused by high-temperature wildfires during the end-Permian mass extinction. Earth and Planetary Science Letters, vol. 614, 118193.
https://doi.org/10.1016/j.epsl.2023.118193

Johnson, C.L., Amory, J.A., Zinniker, D., Lamb, M.A., Graham, S.A., Affolter, M., Badarch, G. 2007. Sedimentary response to arc-continent collision, Permian, southern Mongolia. In: Draut, A., Clift, P., Scholl, D. (Eds.), Formation and Applications of the Sedimentary Record in Arc Collision Zones. Geological Society of America, Special Paper 436, p. 1-26.
https://doi.org/10.1130/2008.2436(16)

Kozlovsky, Y.A. 1984. The Superdeep Well of the Kola Peninsula. Moscow, Ministry of Geology of the USSR, 558 p.

Lanci, L., Galeotti, S., Ratcliffe, K., Tohver, E., Wilson, A. Flint, S. 2022. Astronomically forced cycles in Middle Permian fluvial sediments from Karoo Basin (South Africa). Palaeogeography, Palaeoclimatology, Palaeoecology, vol. 596, 110973.
https://doi.org/10.1016/j.palaeo.2022.110973

Li, M., Ogg, J., Zhang, Y., Huang, C., Hinnov, L., Chen, Z-Q., Zou, Z. 2016. Astronomical tuning of the end-Permian extinction and the Early Triassic Epoch of South China and Germany. Earth and Planetary Science Letters, vol. 441, p. 10-25.
https://doi.org/10.1016/j.epsl.2016.02.017

Longley, I.M., Barraclough, R., Bridden, M.A., Brown, S. 1990. Pematang Lacustrine Petroleum Source Rocks from the Malacca Strait PSC, Central Sumatra, Indonesia. IPA Proceedings, vol. 19(1), p. 279-297.

Lu, J., Wang, Y., Yang, M., Zhang, P., Bond, D., Shao, L., Hilton, J. 2022. Diachronous end-Permian terrestrial ecosystem collapse with its origin in wildfires. Palaeogeography Palaeoclimatology Palaeoecology, vol. 594, 110960.
https://doi.org/10.1016/j.palaeo.2022.110960

Ma, J., Huang, Z., Liang, S., Liu, Z. Liang, H. 2016. Geochemical and tight reservoir characteristics of sedimentary organic-matter-bearing tuff from the Permian Tiaohu Formation in the Santanghu Basin, Northwest China. Marine and Petroleum Geology, vol. 73, p. 405-418.
https://doi.org/10.1016/j.marpetgeo.2016.03.017

Manankov, I.N. 1998. Late Permian Productida (Brachiopoda) from southeastern Mongolia. Paleontological Journal, vol. 32, p. 486-492.

Manankov, I.N. 1999. Reference section and upper Permian zonation in Southeastern Mongolia. Stratigraphy and Geological Correlation, vol. 7(1), p. 56-65.

Manankov, I.N. 2012. Brachiopods, biostratigraphy, and correlation of the Permian marine deposits of Mongolia. Paleontological Journal, vol. 46(12), p. 1325-1349.
https://doi.org/10.1134/S0031030112120040

Manankov, I.N., Shi, G.R., Shen, S.Z. 2006. An overview of Permian marine stratigraphy and biostratigraphy of Mongolia. Journal of Asian Earth Sciences, vol. 26(3-4), p. 294-303.
https://doi.org/10.1016/j.jseaes.2005.11.008

Mays, C., Mcloughlin, S. 2022. End-Permian burnout: the role of Permian-Triassic wildfires in extinction, carbon cycling, and environmental change in eastern Gondwana. Palaios, vol. 37(6), p. 292-317.
https://doi.org/10.2110/palo.2021.051

McMillan, M., Sim, S.J., Wilson, C.R. 2025. Reactive thermodynamics of crustal eclogitization and foundering. Earth and Planetary Science Letters, vol. 658, 119302.
https://doi.org/10.1016/j.epsl.2025.119302

Miall, A. D. 2006. The Geology of Fluvial Deposits: Sedimentary Facies, Basin Analysis, and Petroleum Geology. 4th edition, Berlin, Springer-Verlag, 582 p.
https://doi.org/10.1007/978-3-662-03237-4

Miall, A. D., 2022. Facies Analysis. In: Miall, A.D. (Ed.), Stratigraphy: A Modern Synthesis. Springer Textbooks in Earth Sciences, Geography and Environment. Springer, Cham, p. 91-174.
https://doi.org/10.1007/978-3-030-87536-7_3

Michaelsen, P. 2002. Mass extinction of peat-forming plants and the effect on fluvial styles across the Permo-Triassic boundary, Bowen Basin, Australia. Palaeogeography, Palaeoclimatology, Palaeoecology, vol. 179)3-4), p. 173-188. https://doi.org/10.1016/S0031-0182(01)00413-8

Michaelsen, P. 2016. Late Permian coal formation under boreal conditions along the shores of the Mongol-Transbaikalian seaway. New Concepts in Global Tectonics Journal, vol. 4(4), p. 615-636.

Michaelsen, P., Demberelsuren, B. 2024. Petro-chemical characterization and depositional setting of a late Permian high ash coal deposit, Central Mongolia. Mongolian Geoscientist, vol. 29(58), p. 55-79. https://doi.org/10.5564/mgs.v29i58.3448

Michaelsen, P., Henderson, R.A. 2000. Sandstone petrofacies expressions of multiphase basinal tectonics and arc magmatism: Permian-Triassic north Bowen Basin, Australia. Sedimentary Geology, v. 136, p. 113-136. https://doi.org/10.1016/S0037-0738(00)00090-7

Michaelsen, P., Henderson, R.A., Crosdale, P.J., Mikkelsen, S.O. 2000. Facies architecture and depositional dynamics of the Upper Permian Rangal Coal Measures, Bowen Basin, Australia. Journal of Sedimentary Research, vol. 70(4), p. 879-895. https://doi.org/10.1306/2DC4093F-0E47-11D7-8643000102C1865D

Michaelsen, P., Storetvedt, K.M. 2023. Tectonic evolution of a sequence of related late Permian transtensive coal-bearing subbasins, Mongolia: A global wrench tectonics portrait. Mongolian Geoscientist, vol. 28, p. 1-53. https://doi.org/10.5564/mgs.v28i57.3200

Michaelsen, P., Storetvedt, K.M. 2024. Protracted destabilization and collapse of peat mire ecosystems at the Permo-Triassic boundary recorded by a sequence of related transtensive sub-basins in central and southern Mongolia. Permophiles, vol. 76, p. 46-51.

MNS GB/T 212, 2015. Mongolian standard. Proximate analysis of coal. Methods of determining moisture, ash, and volatile matter contents. 17 p.

MNS ISO 351, 2001. International Standard. Method of determining sulfur content. 5 p.

Nagy, J., Foster, W.J., Svensen, H.H., Planke, S. 2026. Permian-Triassic mass extinction and its aftermath in Boreal waters reflected by foraminifera from Spitsbergen, Palaeogeography, Palaeoclimatology, Palaeoecology, vol. 690, 113698. https://doi.org/10.1016/j.palaeo.2026.113698

Orolmaa, D., Uranbileg, L., Badarch, G. 1999. Stratigraphic questions of coal-bearing deposits in the vicinity of the spring Yamaan-Us bulag. Mongolian Geoscientist, vol. 14, p. 2-8.

Pemberton, S.G., Frey, R.W. 1982. Trace fossil nomenclature and the Planolites-Palaeophycus dilemma. Journal of Paleontology, vol. 56(4), p. 843-881.

Peters, S.E., Gaines, R.R. 2012. Formation of the ‘Great Unconformity’ as a trigger for the Cambrian explosion. Nature, vol. 484, p. 363-366. https://doi.org/10.1038/nature10969

Pickel, W., Kus, J., Flores, D., Kalaitzidis, S., Christanis, K., Cardott, B.J., Misz-Kennan, M., Rodrigues, S., Hentschel, A., Hamor-Vido, M., Crosdale, P., Wagner, N., ICCP. 2017. Classification of liptinite - ICCP System 1994. International Journal of Coal Geology, vol. 169, p. 40-61. https://doi.org/10.1016/j.coal.2016.11.004

Ragon, C., Vérard, C., Kasparian J., Nowak, H., Kustatscher, E., Brunetti, M. 2025. Comparison between plant fossil assemblages and simulated biomes across the Permian-Triassic Boundary. Frontiers in Earth Science, vol. 13, 1520846. https://doi.org/10.3389/feart.2025.1520846

Reading, H.G. 1996. Sedimentary Environments: Processes, Facies and Stratigraphy. 3rd Edition, Blackwell, Oxford, 689 p.

Retallack, G.J., 1995. Permian-Triassic life crisis on land. Science, vol. 267(5194), p. 77-80. https://doi.org/10.1126/science.267.5194.77

Ruditch, E.M.1990. The World Ocean Without Spreading. Shallow-Water Facies of the World Ocean. In: Critical Aspects of the Plate Tectonic Theory. Athens, Greece, Theophrastus Publications, p. 343-395.

Shao, L., Zhang, P., Gayer, R.A., Chen, J. Dai, S. 2003. Coal in a carbonate sequence stratigraphic framework: the Upper Permian Heshan Formation in central Guangxi, southern China. Journal of the Geological Society, vol. 160(2), p. 285-298.

https://doi.org/10.1144/0016-764901-108
Shen, S.-Z., Ramezani, J., Chen, J., Cao, C-Q., Erwin, D.H., Zhang, H., Xiang, L., Schoepfer, S.D., Henderson, C.M., Zheng, Q-F., Bowring, S.A., Wang, Y., Li, X-H., Wang, X-D., Yuan, D-X., Zhang, Y-C., Mu, L., Wang, J., Wu, Y-S. 2018. The sudden end-Permian mass extinction in South China. GSA Bulletin, vol. 131 (1-2), p. 205-223. https://doi.org/10.1130/B31909.1
Singh, I.B. 1980. The Sedimentary Environment of the Gangetic Plain. In: Reineck, H-E., Singh, I.B. (Eds.) Depositional Sedimentary Environments: With Reference to Terrigenous Clastics, Second edition, Springer Verlag, 551 p. https://doi.org/10.1007/978-3-642-81498-3
Sodnomsambuu, D., Klyuchevskii, A.V. 2017. Lithospheric stress in Mongolia, from earthquake source data. Geoscience Frontiers, vol. 8(6), p. 1323-1337. https://doi.org/10.1016/j.gsf.2017.01.003
Song, Y., Tian, Y., Yu, J., Algeo, T.J., Luo, G., Chu, D., Xie, S. 2022. Wildfire response to rapid climate change during the Permian-Triassic biotic crisis. Global and Planetary Change, vol. 215, 103872. https://doi.org/10.1016/j.gloplacha.2022.103872
Storetvedt, K.M. 1990. The Tethys Sea and the Alpine-Himalayan orogenic belt; mega-elements in a new global tectonic system. Physics of the Earth and Planetary Interiors, vol. 62(1-2), p. 141-184. https://doi.org/10.1016/0031-9201(90)90198-7
Storetvedt, K.M. 2003/23. Global Wrench Tectonics: Theory of Earth Evolution. Bergen, Fagbokforlaget, 397 p. https://www.storetvedt.com/book-global-wrench-tectonics-online-edition-2023/
Storetvedt, K.M. 2025. Worldwide distribution of the Glossopteris lineage - The significance of crustal and seawater events. Mongolian Geoscientist, vol. 30(61), p. 94-119. https://doi.org/10.5564/mgs.v30i61.4600
Storetvedt, K.M. 2026. North Atlantic palaeogeography - An extended perspective. Journal of Palaeogeography, vol. 15(4), 100384 https://doi.org/10.1016/j.jop.2026.100384
Storetvedt, K.M., Michaelsen, P. 2024. Sedimentary basins, hydrocarbons, graphite, coal, and Cu-Au deposits - from Mongolia to the Pacific margin: Interplay between the ubiquitous orthogonal fracture network and Global Wrench Tectonics. Mongolian Geoscientist, vol. 29(58), p. 19-54. https://doi.org/10.5564/mgs.v29i58.3234
Tang, H., Zhao, Q., Liu, B., Tan, S., Shi, K. 2023. Types and Genesis of Siderite in the Coal-Bearing Beds of the Late Permian Xuanwei Formation in Eastern Yunnan, China. Minerals, vol. 13(9), 1233. https://doi.org/10.3390/min13091233
Taylor, E.L., Ryberg, P.E. 2007. Tree growth at polar latitudes based on fossil tree ring analysis. Palaeogeography, Palaeoclimatology, Palaeoecology, vol. 255(3-4), p. 246-264. https://doi.org/10.1016/j.palaeo.2007.06.013
Umbgrove, J.H.F. 1942/1947. The Pulse of the Earth. The Hague, Martinus Nijhoff, 380 p. https://doi.org/10.1007/978-94-017-5902-1
Underdown, R., Redfern, J., Lisker, F. 2007. Constraining the burial history of the Ghadames Basin, North Africa: an integrated analysis using sonic velocities, vitrinite reflectance data and apatite fission track ages. Basin Research, vol. 19(4), p. 557-578. https://doi.org/10.1111/j.1365-2117.2007.00335.x
Uranbileg, L. 2003. The new plants of Upper Permian coal deposits in southern Mongolia. Mongolian Geoscientist, vol. 23, p. 47-50
Vajda, V. McLoughlin, S., Mays, C., Frank, T.D., Fielding, C.R., Tevyaw, A., Lehsten, V., Bocking, M., Nicoll, R.S. 2020. End-Permian (252 Mya) deforestation, wildfires and flooding-An ancient biotic crisis with lessons for the present. Earth and Planetary Science Letters, vol. 529, 115875. https://doi.org/10.1016/j.epsl.2019.115875
Vakhrameev, V.A., Lebedev, Y.L., Sodov, Z. 1986. A cycad(?) Guramsania gen. nov. from the Upper Permian of South Mongolia. Paleontological Journal, vol. 20, p. 95-101.
Van Iten, H. 1991. Evolutionary affinities of conulariids, in Simonetta. In: A.M., Morris, S.C., (Eds.). The Early Evolution of Metazoa and the Significance of Problematic Taxa. Cambridge University Press, Cambridge. p. 145-155.
Van Wagoner, J.C., Mitchum, R.M., Campion, K.M., Rahmanian, V.D. 1990. Siliciclastic Sequence Stratigraphy in Well Logs, Cores

and Outcrops. Concepts for High-Resolution Correlation of Time and Facies. AAPG Methods in Exploration Series, vol. 7, 55 p. https://doi.org/10.1306/Mth7510

Wang, K., Lu, X., Liu, X., Zhou, M., Yin, K. 2022. Partitioning of noble gases (He, Ne, Ar, Kr, Xe) during Earth's core segregation. Geochimica et Cosmochimica Acta, vol. 321, p. 329-342. https://doi.org/10.1016/j.gca.2022.01.009

Waterhouse, J.B. 1979. Permian and Triassic conulariid species from New Zealand. Journal of the Royal Society of New Zealand, vol. 9(4), p. 475-489. https://doi.org/10.1080/03036758.1979.10421833

Wegener, A. 1929/66. The Origin of Continents and Oceans. London, Methuen & Co. Ltd., 248 p.

Wentworth, C. R., 1922. A Scale of Grade and Class Terms for Clastic Sediments. Journal of Geology, vol. 30(5), p. 377-392. https://doi.org/10.1086/622910

Xie, S. 2024. Mass extinctions, their causes and consequences; an interview with Douglas H. Erwin and Shuzhong Shen. National Science Review, vol. 11(1), nwad250. https://doi.org/10.1093/nsr/nwad250

Zhang, P., Yang, M., Lu, J., Bond, D.P.G., Zhou, K., Xu, X., Wang, Y., He, Z., Bian, X., Shao, L., Hilton, J. 2023. End-Permian terrestrial ecosystem collapse in North China: Evidence from palynology and geochemistry. Global and Planetary Change, vol. 222, 104070. https://doi.org/10.1016/j.gloplacha.2023.104070

Zinniker, D.A. Badarch, G. 1997. Reconnaissance palynology and evidence of climate change across the Permian/Triassic boundary, Ih Uvgon, southern Mongolia: Geological Society of America Abstracts with Programs, vol. 29(6), p. 97.

Shcherbakov, D.E. 2008. On Permian and Triassic insect faunas in relation to biogeography and the Permian-Triassic crisis. Paleontological Journal, vol. 42, p. 15-31. https://doi.org/10.1134/S0031030108010036

APPENDIX TABLE 1

Sample #	Northing	Easting	Thin Section #
1	42° 52' 15.4" N	105° 30' 58.5" E	TTT01
2	42° 52' 14.3" N	105° 30' 59.0" E	TTT02
3	42° 52' 06.1" N	105° 30' 26.2" E	TTT03
4	42° 52' 05.8" N	105° 29' 23.5" E	TTT04
5	42° 51' 46.9" N	105° 29' 01.7" E	TTT05
6	42° 52' 02.1" N	105° 28' 14.1" E	TTT06
7	42° 52' 29.0" N	105° 35' 17.0" E	TTT07
8	42° 52' 25.2" N	105° 34' 05.7" E	TTT08
9	42° 52' 20.4" N	105° 33' 34.3" E	TTT09
10	42° 52' 16.6" N	105° 32' 37.1" E	TTT10
11	42° 52' 05.0" N	105° 29' 23.0" E	TTT11

APPENDIX TABLE 2

Seam #	Moisture (ad)	Ash (db)	Volatiles (daf)	Sulphur (db)	CV (daf)	Density (gr/cm^3)	C (%)	H (%)	N (%)	O_2 (%)
7	0.27-9.7	3.41-74.36	34.7-35.65	0.32-2.91	6922.22-7906.11	1.38-1.46	74.24	4.41	1.89	6.95
	5.519 (67)	13.53(67)	35.07(67)	0.88 (67)	7278.43 (30)	1.39 (67)	74.24 (30)	4.41(30)	1.89 (30)	6.95 (30)
6	0.35-8.08	5.43-76.48	35.27-35.27	0.29-1.22	7241.67-7965	1.33-1.33	70.75-75.98	4.50-4.60	1.84-1.92	7.35-7.99
	4.84 (51)	17.6(51)	35.27(51)	0.69 (51)	7840.4 (51)	1.33 (51)	73.37 (31)	4.55(31)	1.88 (31)	7.76 (31)
5	1.16-9.00	6.62-49.91	25.91-33.81	0.21-1.22	6483-7496.11	1.45-1.75	40.22	2.15	1.08	6.2
	4.9 (31)	20.77(31)	31.64(31)	0.72 (31)	6725.12 (8)	1.54 (31)	40.22 (8)	2.15(8)	1.08 (8)	6.2 (8)
4R	0.48-9.50	4.94-64.19	17.88-35.22	0.16-0.95	6576.11-6576.11	1.33-1.89	66.97	4.95	1.86	10.83
	4.48 (47)	19.63 (47)	26.78 (47)	0.46 (47)	6576.11 (18)	1.62 (18)	66.97 (17)	4.95(17)	1.86 (17)	10.83 (17)
4U-4L	0.27-8.30	6.19-61.11	28.82-30.83	0.27-5.97	7750-7750	1.32-1.6	67.33	4.94	1.99	9.88
	4.12 (89)	15.97 (89)	30.04 (51)	0.67 (89)	7750 (27)	1.44 (51)	67.33 (27)	4.94(27)	1.99 (27)	9.88 (27)
4A	9-9	10.14-19.66	31.92-31.92	0.73-0.99	6206.67-7906.11	1.41-1.41	66.08-73.58	3.70-4.28	1.78-1.86	7.81-8.05
	9 (6)	15.45 (6)	31.92 (6)	0.8 (6)	7012.55 (6)	1.41 (6)	69.83 (22)	3.99(22)	1.82 (22)	7.93 (22)
3M	2.45-7.5	22.39-40.66	24.64-24.64	0.22-1	5515-7933.14	1.53-1.53	58.11	2.76	1.39	7.57
	6.9 (15)	29.31 (15)	24.64 (15)	0.59 (15)	6314.55 (15)	1.53 (15)	58.11 (12)	2.76(12)	1.39 (12)	7.57 (12)
3RU	1.25-6.90	17.57-40.04	24.76-24.76	0.21-0.51	6117.78-6117.78	1.47-1.47	66.40	3.30	1.64	4.75
	4.96 (17)	22.88 (17)	24.76 (17)	0.44 (17)	6117.78 (10)	1.47 (10)	66.4 (9)	3.3(9)	1.64 (9)	4.75 (9)
3RL	1.2-9.9	16.02-44.94	26.64-26.64	0.25-0.47	7672.22-7820	1.51-1.51	-	-	-	-
	6.21 (7)	23.7 (13)	26.64 (7)	0.32 (13)	7772.2 (6)	1.51 (2)	-	-	-	-
3U	1-6.7	19.34-53.28	22.63-28.19	0.11-0.43	7609.44-7609.44	1.57-1.76	-	-	-	-
	1.25 (19)	33.68 (12)	25.41 (4)	0.34 (19)	7609.44 (7)	1.66 (4)	-	-	-	-
3	1.37-8	13.05-47.68	29.49-29.49	0.26-0.87	7609.44-7732.22	1.47-1.47	-	-	-	-
	4.08 (9)	24.91 (18)	29.49 (6)	0.5 (18)	7615.65 (9)	1.47 (6)	-	-	-	-
3L	-	50.59-50.76	-	0.51-0.95	7097.78-7488.33	-	-	-	-	-
	-	50.68 (6)	-	0.71 (6)	7275.92 (6)	-	-	-	-	-
2D	0.3-5.5	16.07-42.44	20.53-25.20	0.18-0.38	-	1.61-1.73	-	-	-	-
	3.92 (23)	26.78 (23)	22.42 (23)	0.31 (12)	-	1.64 (12)	-	-	-	-
2C	0.57-1.15	44.93-45.85	-	0.36-0.46	-	-	-	-	-	-
	0.93 (7)	45.51 (7)	-	0.39 (7)	-	-	-	-	-	-
2B	0.81-1.72	21.81-47.89	18.31-18.31	0.4-0.47	-	1.79-1.79	-	-	-	-
	1.09 (5)	34.18 (8)	18.31 (2)	0.44 (8)	-	1.79 (2)	-	-	-	-
1U	0.55-6.6	21.00-55.54	21.22-25.56	0.16-2.79	2738.88-6157.77	1.42-1.62	51.62-60.27	2.15-3.30	1.19-1.60	5.38-7.89
	7.16 (99)	31.52 (246)	23.73 (108)	0.92 (246)	4980.83 (167)	1.56 (109)	54.94(158)	2.72(158)	1.37(158)	6.33(158)
1U-1L	0.19-13.5	20.1-62.16	16.25-25.45	0.1-2.41	3097.22-9524	1.44-2.16	41.32-60.29	2.12-2.99	0.94-1.56	4.84-6.37
	4.17 (393)	31.27 (469)	23.85 (366)	0.55 (469)	5976.49 (434)	1.62 (434)	53.61(238)	2.63(238)	1.35(238)	5.60(238)
1L	0.63-5.8	18.04-39.84	23.43-23.43	0.44-1.72	5121.11-8011.11	1.58-1.58	49.20-54.96	2.26-2.69	1.19-1.36	5.06-5.81
	5.27 (49)	27.81 (116)	23.43 (43)	0.91 (116)	6401.23 (43)	1.58 (43)	52.08(85)	2.48(85)	1.28(85)	5.44(85)
0	0.83-7.34	27.45-71.63	31.04-67.34	0.32-1.82	4934.09-8652.83	-	-	-	-	-
	2.71 (36)	39.3 (36)	38 (36)	1.13 (36)	7366.71 (36)	-	-	-	-	-

APPENDIX TABLE 3

Seam #	SiO_2 (%)	Al_2O_3 (%)	CaO (%)	Fe_2O_3 (%)	MgO (%)	SO_3 (%)	TiO_2 (%)	P_2O_3 (%)	K_2O (%)	Na_2O (%)	Mn_2O_3 (%)	BaO (%)	SrO (%)
7	50.94	13.03	10.53	13.12	3.18	6.88	0.48	0.82	0.13	0.34	0.22	0.07	0.17
6	58.3	23.47	2.03	9.35	1.29	1.82	1	0.18	0.56	0.34	0.07	1.12	0.09
5	44.1	12.81	16.31	11.15	6.44	7.08	0.53	1.48	0.58	0.49	0.13	0.24	0.23
4R	63.26	20.54	3.35	4.33	2.17	2.08	0.98	0.58	1.27	0.53	0.02	0.08	0.13
4U-4L	58.61	18.28	5.97	6.5	3.27	5.75	0.64	0.32	0.43	0.5	0.08	0.08	0.12
4A	52.67	18.51	8.23	7.36	3.9	6.35	0.55	1.23	0.38	0.21	0.11	0.21	0.31
3M	67.08	19.48	0.63	9.8	0.43	0.19	0.78	0.09	1.02	0.15	0.14	0.16	0.05
3RU	74.19	18.88	0.57	3.86	0.39	0.27	0.67	0.09	0.7	0.13	0.05	0.15	0.05
3RL	65.3	16.6	3.7	7.8	0.7	0.1	0.66	3.12	0.27	0.63	0.05	0.15	0.11
3U	60.1	14.7	11.6	6.5	2.44	1.14	0.69	0.3	0.95	1	0.11	0.07	0.08
3	59.6	14.8	14.2	3.68	2.8	2.85	0.54	0.68	0.34	0.57	0.05	0.04	0.18
2D	74.6	20	0.91	1.1	0.52	0.39	0.72	0.38	0.7	0.15	0.01	0.06	0.06
2C	68.3	20.9	2	3.36	1.47	1.03	0.62	0.65	1.03	0.16	0.01	0.11	0.1
2B	71.95	22.55	0.6	1.05	0.45	0.15	1.12	0.66	1.25	0.19	0.005	0.16	0.15
1U	71.15	16.17	3.67	3.27	1.08	2.36	0.56	0.77	0.45	0.15	0.05	0.23	0.1
iU-1L	71.21	16.47	3.91	3.32	1.07	2.11	0.57	0.46	0,55	0,13	0.06	0.15	0.09
1L	69.07	19.01	2.36	4.1	0.64	1.37	0.67	0.35	0.5	0.11	0.14	0.15	0.06

APPENDIX TABLE 4

Seam	Vitrinite %	Liptinite %	Inertinite %	Mineral Matter %	Semifusinite %	Total %	Rr Random	RoMax (measured)
Seam 7	69	0	5	25	1	100	0.372	0.424
Seam 6	41	3	38	6	12	100	0.611	0.663
Seam 6	46	5	29	6	14	100	0.614	0.666
Seam 6	38	12	30	8	12	100	0.586	0.638
Seam 5	49	7	24	14	6	100	0.493	0.545
Seam 5	35	2	38	13	12	100	0.49	0.542
Seam 4	42	3	36	10	9	100	0.632	0.684
Seam 4	42	7	34	7	10	100	0.628	0.68
Seam 4	46	4	31	8	11	100	0.676	0.728
Seam 4	54	2	28	8	8	100	0.669	0.721
Seam 4	59	4	24	4	9	100	0.682	0.734
Seam 4	47	4	33	7	9	100	0.648	0.7
Seam 2	31	0	24	18	27	100	0.719	0.771
Seam 2	41	0	29	14	16	100	0.686	0.738
Seam 2	52	0	22	9	17	100	0.724	0.776
Seam 1							0.794	0.847